



HAL
open science

First experimental determination of the solubility constant of coffinite

Stephanie Szenknect, Adel Mesbah, Théo Cordara, Nicolas Clavier, H.P. Brau, X. F Le Goff, Christophe Poinssot, Rodney Ewing, Nicolas Dacheux

► **To cite this version:**

Stephanie Szenknect, Adel Mesbah, Théo Cordara, Nicolas Clavier, H.P. Brau, et al.. First experimental determination of the solubility constant of coffinite. *Geochimica et Cosmochimica Acta*, 2016, 181, pp.36-53. 10.1016/j.gca.2016.02.010 . hal-01998419

HAL Id: hal-01998419

<https://hal.science/hal-01998419>

Submitted on 25 Apr 2019

HAL is a multi-disciplinary open access archive for the deposit and dissemination of scientific research documents, whether they are published or not. The documents may come from teaching and research institutions in France or abroad, or from public or private research centers.

L'archive ouverte pluridisciplinaire **HAL**, est destinée au dépôt et à la diffusion de documents scientifiques de niveau recherche, publiés ou non, émanant des établissements d'enseignement et de recherche français ou étrangers, des laboratoires publics ou privés.

First experimental determination of the solubility constant of coffinite.

Stephanie Szenknect^{†*}, Adel Mesbah[†], Théo Cordara[†], Nicolas Clavier[†], Henri-Pierre Brau[†], Xavier Le Goff[†],
Christophe Poinssot[§], Rodney C. Ewing[‡] and Nicolas Dacheux[†].

[†] ICSM, UMR 5257 CEA/CNRS/UM2/ENSCM, Site de Marcoule – Bât. 426, BP 17171, 30207 Bagnols-sur-Cèze cedex, France

[‡] Department of Geological Sciences, Stanford University, Stanford, CA 94305-2115 USA

[§] CEA, Nuclear Energy Division, RadioChemistry & Processes Department, CEA Marcoule, Bât. 400, BP 17171, 30207 Bagnols-sur-Cèze cedex, France

KEYWORDS. coffinite, uranium silicate, solubility constant, uraninite, silica, coffinitization.

ABSTRACT.

Dissolution experiments have been performed in order to determine the solubility constant of coffinite, USiO_4 . Several assemblages of phases were used in under-saturated experiments performed in 0.1 mol L^{-1} HCl under Ar atmosphere, as well as in air. These samples were fully-characterized and were composed of either USiO_4 , solely, or USiO_4 and additional oxide byproducts that resulted from the synthesis procedure. The solubility constant of coffinite was determined at 25°C and 1 bar ($\log {}^*K_S^\circ(\text{USiO}_4, \text{cr}) = -5.25 \pm 0.05$), as well as the standard free energy of formation of coffinite ($\Delta_f G^\circ(298 \text{ K}) = -1867.6 \pm 3.2 \text{ kJ mol}^{-1}$), which enables one to infer the relative stability of coffinite and uraninite as a function of groundwater composition. Geochemical simulations using PHREEQC 2 software and the Thermochimie data base indicate that coffinite precipitates at 25°C under reducing conditions, at $\text{pH} = 6$, for $\text{H}_4\text{SiO}_4(\text{aq})$ concentration of $7 \cdot 10^{-5} \text{ mol L}^{-1}$ and $\text{U}(\text{OH})_4(\text{aq})$ concentration of $10^{-11} \text{ mol L}^{-1}$. The $\Delta_f G^\circ$

*Author to whom correspondence should be addressed: stephanie.szenknect@cea.fr

value determined was used to calculate the standard free energy associated with the formation of coffinite from a mixture of uraninite and quartz. The value obtained ($\Delta_{r,ox}G^\circ = 20.6 \pm 5.2 \text{ kJ mol}^{-1}$) indicates unambiguously that coffinite is less stable than the quartz + uraninite mixture at 25°C. Geochemical simulations using PHREEQC 2 software indicate that coffinite precipitates in solutions supersaturated with respect to $\text{UO}_2(\text{cr})$, but undersaturated with respect to $\text{UO}_2(\text{am})$ in aqueous solutions with silica concentrations typical of groundwater. These favorable conditions during the formation of sedimentary uranium ore deposits, as well as slow dissolution kinetics, explain the common occurrence of coffinite.

1. INTRODUCTION

The direct disposal of spent nuclear fuel (SNF) in underground geological repositories is one of the main options pursued in a number of countries, such as Sweden, Finland, Switzerland and USA (Hogselius, 2009). Over time in a geologic repository, and after the early, rapid release of radionuclides that are at grain boundaries, the Instant Release Fraction (IRF), fission products and actinides dissolved in the UO_2 matrix will be more slowly released by dissolution of the UO_2 grains in the spent fuel after degradation of engineered barriers, such as the backfill and waste package (Poinssot et al., 2005). Secondary phases that form during SNF dissolution could become important sinks for uranium and other radionuclides and could control the subsequent mobility and the ultimate distribution of radiotoxic elements in the environment (Baker, 2014; Gorman-Lewis et al., 2008; Maher et al., 2012). Except for the Yucca Mountain site in the USA, most of the geologic sites under investigation for an underground repository are located in undisturbed clay-rich rock or granite, with silica-rich groundwaters, deep enough to have reducing conditions. For instance, pore-water samples collected at a depth of 490 m in Callovo-Oxfordian clayrock, in the Bure (France) underground research laboratory exhibited near neutral pH (7.2 ± 0.2), low redox potential ($E_{\text{hSHE}} = -199$ mV) and Si concentration ($1.4 \cdot 10^{-4}$ mol L^{-1}), high enough to allow silica precipitation (Gaucher et al., 2009). Granitic groundwater collected at a depth of 510 m in Forsmark and Äspö crystalline bedrock (Sweden) exhibited Si concentration of $1.8 \cdot 10^{-4}$ mol L^{-1} and $1.5 \cdot 10^{-4}$ mol L^{-1} , respectively (Carbol et al., 2012). If coffinite is a less soluble phase than $\text{UO}_2(\text{s})$ under these conditions, it may precipitate and trap the tetravalent uranium released from the SNF (Amme et al., 2005; Hemingway, 1982; Janeczek and Ewing, 1992a, b; Langmuir, 1997). Such a process was already proposed based on observations of the natural nuclear reactors at Oklo and Oklobondo (Gabon), where uraninite, $\text{UO}_2(\text{cr})$ was observed to be altered to coffinite (Janeczek, 1999). In order to evaluate the likelihood of coffinitization of the UO_2 matrix, the thermodynamic data associated with the following reaction must be known:



However, the thermodynamic data for reaction (1) remain poorly constrained. The few data reported in the literature were estimated by analogy with thorite (ThSiO_4) (Brookins, 1975) or from available geologic information. In 1978, Langmuir first postulated that the average silica concentration (about 10^{-3} mol $\cdot \text{L}^{-1}$) found in groundwater draining the Grants Mineral Belt in New Mexico (USA), where both uraninite and coffinite occur in the ore deposits, represents a good estimate of the equilibrium silica activity for reaction (1). This inference was based on field evidence that is the common occurrence of uraninite with quartz in ore deposits, and the concentration of silica in

29 associated groundwaters. Thus, Langmuir estimated the standard free energy of formation of coffinite ($\Delta_f G^\circ(\text{USiO}_4$,
30 cr) = -1891.17 kJ mol⁻¹) and of the enthalpy of formation ($\Delta_f H^\circ(\text{USiO}_4$, cr) = -2001.21 kJ mol⁻¹). However, these
31 values were corrected later by Langmuir and Chatham (1980). The corresponding corrected free energy and enthalpy
32 values were -1882.38 kJ mol⁻¹ and -1990.33 kJ mol⁻¹, respectively (Langmuir, 1978). They also calculated the
33 standard molar entropy of coffinite ($S_m^\circ = 117.15$ J mol⁻¹ K⁻¹) as the sum of the molar entropies of quartz (41.46 J mol⁻¹
34 K⁻¹) and uraninite (77.03 J mol⁻¹ K⁻¹). These values are CODATA values (Cox et al., 1989), which were also used
35 later by Grenthe (1992). In 1982, Hemingway performed thermodynamic calculations, also based on an estimate of
36 the silica activity at equilibrium, for the coffinitization reaction ($(\text{H}_4\text{SiO}_4) = 2.6 \cdot 10^{-4}$), and derived a value for the
37 standard free energy of formation of coffinite ($\Delta_f G^\circ(\text{USiO}_4$, cr) = -1886 ± 20 kJ mol⁻¹). Hemingway indicated that the
38 $\Delta_f G^\circ(\text{USiO}_4$, cr) value given by Langmuir (1978) was not consistent with his estimate for the equilibrium silicate
39 activity for reaction (1). The NEA Thermodynamic Data Base (TDB) (Grenthe et al., 1992) accepted Langmuir's
40 assumption for the average silica concentration (10⁻³ mol L⁻¹) at equilibrium for reaction (1) but recalculated the
41 $\Delta_f G^\circ(\text{USiO}_4$, cr) value and associated error using auxiliary data selected by the NEA-TDB. The obtained value,
42 $\Delta_f G^\circ(\text{USiO}_4$, cr) = -1883.6 ± 4.0 kJ mol⁻¹ was consistent with that of Hemingway. Considering that $S_m^\circ = 118 \pm 12$ J
43 mol⁻¹ K⁻¹, the enthalpy of formation was calculated internally with the Gibbs-Helmholtz equation, leading to
44 $\Delta_f H^\circ(\text{USiO}_4$, cr) = -1991.326 ± 5.367 kJ mol⁻¹. In 1997, Langmuir determined a value for the standard free energy of
45 formation of amorphous coffinite based on chemical analyses of low Eh groundwater from coffinite-bearing ore zones
46 (Cigar Lake, Canada and Palmottu, Finland). These waters were found to be at saturation with respect to UO₂(am),
47 suggesting that the associated coffinite phase may be amorphous. This calculation is the basis for the determination of
48 $\Delta_f G^\circ(\text{USiO}_4$, am) = -1835.23 kJ mol⁻¹. Naturally occurring coffinite is generally so fine-grained that identification and
49 characterization, as well as the determination of physical and chemical properties, is not possible (Deditius et al.,
50 2012; Deditius et al., 2008). Based on Langmuir's interpretation of the geologic conditions of formation, the
51 equilibrium constant of reaction (2) increases by almost 8 orders of magnitude if the coffinite is considered to be
52 amorphous rather than crystalline:



54 Nevertheless, this $\Delta_f G^\circ(\text{USiO}_4$, am) value was mentioned, but not selected for the NEA Thermodynamic Data
55 Base II (Guillaumont et al., 2003) because the solid phase was not identified; thus, there was no established

56 composition; specifically, the presence of molecular water in the structure was not determined. Hence, it is not
57 possible to report a $\Delta_f G^\circ$ value for this amorphous coffinite.

58 Fleche, (2002) derived thermodynamical functions for coffinite using *ab initio* calculations. The $\Delta_f H^\circ(\text{USiO}_4,$
59 cr) value obtained reaches $-2021.7 \pm 30.3 \text{ kJ mol}^{-1}$, using $S_m^\circ = 124.3 \pm 6.6 \text{ J mol}^{-1} \text{ K}^{-1}$ also given in Fleche (2002), it
60 was possible to deduce $\Delta_f S^\circ(\text{USiO}_4, \text{cr}) = -355 \pm 7 \text{ J K}^{-1} \text{ mol}^{-1}$, then the Gibbs-Helmholtz equation led to the
61 determination of $\Delta_f G^\circ(\text{USiO}_4, \text{cr}) = -1915.9 \pm 32.4 \text{ kJ mol}^{-1}$.

62 By extrapolation from the uranothorite solid-solution binary, Szenknect et al. (2013) determined a value for the
63 equilibrium constant of reaction (2): $\log *K_S^\circ(\text{USiO}_4, \text{cr}) = -6.1 \pm 0.2$, which was higher than the estimate based on
64 Langmuir's assumptions of geologic conditions. Thermodynamic calculations based on this extrapolation and
65 auxiliary data from the NEA TDB II (Guillaumont et al., 2003) resulted in a standard free energy of formation for
66 coffinite ($\Delta_f G^\circ(\text{USiO}_4, \text{cr}) = -1872.6 \pm 3.8 \text{ kJ mol}^{-1}$). Recently, Guo et al. (2015) determined experimentally the
67 enthalpy of formation of coffinite by high temperature oxide melt solution calorimetry. They found that coffinite is
68 metastable with respect to a mixture of uraninite and quartz by $25.6 \pm 3.9 \text{ kJ mol}^{-1}$. From this $\Delta_{r,ox} H^\circ$ value, they
69 calculated the standard enthalpy of formation of coffinite $\Delta_f H^\circ(\text{USiO}_4, \text{cr}) = -1970.0 \pm 4.2 \text{ kJ mol}^{-1}$. Considering that
70 $S_m^\circ = 118 \pm 12 \text{ J mol}^{-1} \text{ K}^{-1}$ (selected by the NEA), the free energy of formation was calculated internally using the
71 Gibbs-Helmholtz equation: $\Delta_f G^\circ(\text{USiO}_4, \text{cr}) = -1862.3 \pm 7.8 \text{ kJ mol}^{-1}$.

72 Because of the pressing need for more accurate thermodynamic data, such as $*K_S^\circ$, $\Delta_f G^\circ$, $\Delta_f H^\circ$, $\Delta_f S^\circ$, a number
73 of investigators have sought to obtain pure synthetic coffinite, but only few have succeeded (Costin et al., 2011;
74 Fuchs and Gebert, 1958; Fuchs and Hoekstra, 1959; Hoekstra and Fuchs, 1956; Labs et al., 2014; Pointeau et al.,
75 2009). The synthetic coffinite was always obtained by minor modifications of the initial protocol proposed by Fuchs
76 and Hoekstra (1959). This seminal publication already showed the need for several steps to buffer the pH prior to heat
77 treatment and the difficulty of maintaining a very narrow pH range for formation. Nevertheless, the samples obtained
78 were mixtures of phases, mainly composed of USiO_4 , UO_2 and SiO_2 . An optimized protocol was used to obtain pure
79 coffinite that was fully characterized before and after under-saturated experiments. The purpose of this study is to
80 determine the solubility of coffinite and to use these results to calculate the standard free energy of formation of
81 coffinite, which enables one to infer the relative stability of coffinite and uraninite as a function of groundwater

82 composition. The results are interpreted in terms of likelihood of the coffinitization process of SNF and compared to
83 field evidence, such as the occurrence of associated uraninite and coffinite in uranium sandstone deposits.

84

85 2. EXPERIMENTAL METHODS

86 2.1. Synthesis of solid phases

87 A solution of uranium tetrachloride was prepared by dissolving uranium metal fragments provided by CETAMA
88 (Analytical Methods Committee, CEA, France) in cooled 6 mol L⁻¹ HCl according to the method of Dacheux et al.
89 (1995). The hot solution was then centrifuged at 12000 rpm during 15 min while slow H₂ degassing from black
90 residues was observed. The centrifuged solution was stored under Ar atmosphere, then the final concentration was
91 determined by ICP-AES. The other reactants (Na₂SiO₃, NaHCO₃ and NaOH) were used as supplied by Sigma-Aldrich
92 and were of analytical grade.

93 Coffinite (USiO₄) powder was synthesized under hydrothermal conditions by a modification of previous procedure
94 (Fuchs and Gebert, 1958; Fuchs and Hoekstra, 1959; Hoekstra and Fuchs, 1956). 20 mL of out-gassed water (boiled
95 for 1 hour and cooled under nitrogen stream) containing 6 mmol of UCl₄ was mixed to 20 mL of a solution of
96 Na₂SiO₃ (6 mmol + 10% excess) resulting in a greenish solution. Afterward, the pH was raised to 11.4 ± 0.1 by
97 adding 8 mol L⁻¹ NaOH, buffered to 8.7 by adding NaHCO₃, poured in a 50-mL Teflon container that was placed in
98 acid digestion bomb. All these reactions were performed in a glove box filled with Ar and free from oxygen (less than
99 2 ppm). The digestion bomb was then heated at 250 °C for 16 days. At the end of the reaction, the final product was
100 separated by centrifugation twice with water then with ethanol and dried overnight in the glove box at room
101 temperature.

102 In order to evaluate whether the byproducts (oxide and amorphous silica) control the concentrations in solution,
103 another reaction was performed in order to synthesize only these side products. Basically, the same procedure was
104 followed; however, the pH was raised to 12.5 before buffering the pH to 8.7. Mesbah et al. (2015) determined the
105 optimal conditions in terms of pH, T, heating time and molar ratio of U:Si for the hydrothermal synthesis of coffinite.
106 The yield of coffinite was found to decrease drastically when the pH of the initial mixture of reactants was lower than
107 10 or higher than 12. This result was attributed to the formation of colloidal coffinite precursors in a narrow range of
108 pH. Without these colloidal precursors, acting as nuclei for the crystallization of coffinite, the kinetics of coffinite
109 precipitation was too slow to allow the precipitation of a sufficient amount of coffinite.

110

111 2.2. Coffinite purification

112 The powders were purified prior to dissolution experiments in order to eliminate UO_2 and SiO_2 that have been
113 retained in the synthesized powders. The protocol for purification developed for uranothorite solid solutions (Clavier
114 et al., 2013) yielded very high losses for coffinite; thus, the protocol was modified. One purification cycle consisted
115 of several steps: *i.*) 100 mg of solid were placed into contact with 50 mL of 10^{-2} mol L^{-1} HNO_3 for 3 to 5 days; *ii.*) the
116 solid was centrifuged and washed three times with deionized water; *iii.*) the remaining solid was dispersed in 50 mL
117 of 10^{-2} mol L^{-1} KOH for 3 to 5 days, and then washed three times with deionized water. Two or three purification
118 cycles were performed, and the resulting samples were dried overnight in an oven at 60°C .

119

120 2.3. Characterization of the solids

121 All samples were analyzed by powder X-rays diffraction (PXRD) using the Bruker D8 advance diffractometer
122 equipped with a lynx eye detector and $\text{K}_\alpha(\text{Cu})$, $\lambda = 1.54118 \text{ \AA}$. All the data were collected in the reflection geometry
123 in the angular range from 5° to 100° for a total counting time of about 3 hours per sample. Mainly, two phases were
124 detected, tetragonal coffinite (USiO_4 ; $I4_1/amd$) and cubic urania (UO_2 ; $\text{Fm}\bar{3}m$). The data were refined using
125 Fullprof_suite (Frontera and Rodriguez-Carvajal, 2003) by applying the Rietveld method and using the Thomson Cox
126 profile function (Thompson et al., 1987). Pure silicon was used as a standard to determine instrumental parameters.
127 Zero shift, unit cell parameters, overall displacement, preferred orientation and an anisotropic size model for the
128 microstructural characteristics were considered for all refinements. The obtained unit cell parameters and estimated
129 amounts of each phase are reported in Table 2, while an example of the refinement results for pure coffinite is given
130 in Figure S1 of the supplementary data showing the observed, calculated and difference patterns.

131 Low magnification transmission electron microscopy (TEM) analyses were conducted at 200 kV on a Jeol 200CX
132 TEM equipped with a Photonic-Science camera. Samples were first dispersed in absolute ethanol then one drop was
133 deposited on carbon coated grid prior to analysis.

134 Scanning electron microscopy (SEM) analyses were conducted using an FEI Quanta 200 electron microscope
135 equipped either with an Everhart-Thornley detector (ETD) or a backscattered electron detector (BSED) in high
136 vacuum conditions with a low accelerating voltage (2.0 - 3.1 kV). These conditions produced high-resolution images.
137 Small powder samples were then directly analyzed without any additional preparation. X-ray energy dispersive

138 spectroscopy (EDS) analyses were performed using a Bruker AXS X-Flash 5010 detector coupled to the SEM device.
139 In order to quantify the elemental percentages, the powders were first embedded in epoxy resin. The surface of the
140 samples was then polished to optical grade and then carbon coated. Experimental data were finally collected from 100
141 different locations using UO_2 and albite ($\text{NaAlSi}_3\text{O}_8$) as standards.

142 The specific surface area of the solids was measured by nitrogen absorption at 77K using the Brunauer–Emmett–
143 Teller (B.E.T.) method with a TRISTAR 3020 (Micromeritics) apparatus.

144

145 2.4. Solubility experiments

146 The dissolution experiments were performed in air or under anoxic conditions by flushing the chamber with argon.
147 As-prepared, purified samples were used for the dissolution experiments. Respectively, 100 mg or 30 mg of as-
148 prepared or purified samples were introduced in sealed polytetrafluoroethylene (PTFE) jars (Savillex) and placed in
149 contact with 30 mL of $0.10 \text{ mol}\cdot\text{L}^{-1}$ HCl solution prepared by volumetric dilution of concentrated HCl (37 %) from
150 Sigma-Aldrich with deionized water. The solution was then out-gassed for anoxic experiments by boiling it for
151 2 hours and cooling under bubbling with Ar 6.0. The 0.1 M HCl was then stored for several days in the glove box
152 before being used in the dissolution experiments in order to reach equilibrium with the $\text{O}_2(\text{g})$ partial pressure. Using
153 the Henry's law constant provided in the ANDRA thermodynamic database `thermochimie-PHREEQC_SIT_v9`
154 (Giffaut et al., 2014): $\log K_H = 10^{-2.900}$ and the $\text{O}_2(\text{g})$ partial pressure measured in the glove box ($2 \cdot 10^{-6}$ bar), the initial
155 $\text{O}_2(\text{aq})$ concentration in the HCl solution did not exceed $2.5 \cdot 10^{-9} \text{ mol L}^{-1}$. The dissolution reactors were then filled
156 with HCl solution and closed in the glove box. All the experiments were performed in duplicate at $298 \pm 2 \text{ K}$. The
157 dissolution continued for up to several months. During this time, the reactors were stirred at least twice a week and
158 opened only to sample the solution. The dissolution of the solid was then monitored through regular pH
159 measurements using a Metrohm combination-glass electrode calibrated against pH buffers (Inlab® Solutions, Mettler
160 Toledo, pH = 2.00; 4.01 and 7.00 at 25°C), whereas uranium and silicon concentrations in the leachate were measured
161 by inductively coupled plasma atomic emission spectroscopy (ICP-AES). For each sample, 2 mL of the leaching
162 solution was withdrawn and centrifuged at 12,000 rpm for 2 min. These conditions ensured the removal of colloids
163 larger than 10 nm. Then 1.8 mL of the solution was diluted in 4.2 mL of 0.2 mol L^{-1} HNO_3 solution for further ICP-
164 AES analyses using a Spectro Arcos EOP device. For this purpose, the spectrometer was calibrated with SPEX
165 standard solutions. Finally, fresh HCl solution was introduced into the reactors in order to maintain a constant volume

166 of solution in contact with the solid. The volume of the gas phase in the dissolution reactor corresponded to the
167 internal volume of the Teflon screw cap that did not exceed 3 cm³. Thus, each time the reactor was opened in the
168 glove box, the renewed volume of gas contained about 2.5 10⁻¹⁰ moles of O₂(g). The maximum number of samples
169 reached 30, the maximum amount of O₂(g) introduced into the system by solution sampling thus did not exceed 7.5
170 10⁻⁹ moles. The elementary uranium concentration in solution at steady state was in the range between 6.4 10⁻⁵ and
171 2.6 10⁻³ mol L⁻¹. Assuming that the oxidation of aqueous U(IV) by O₂ in the system was complete and that the 7.5 10⁻⁹
172 moles of oxygen entering the system were consumed by U⁴⁺ oxidation in solution, 5 10⁻⁷ mol L⁻¹ of UO₂²⁺ must have
173 formed. This concentration represents a maximum of 0.8 % of the elemental concentration of U. A calculation was
174 performed using the PHREEQC 2 software and the thermochimie_PHREEQC_SIT_v9 database (selected reaction
175 constants are indicated in Table 1) in order to estimate the oxygen fugacity of the gas phase in equilibrium with a HCl
176 0.1 mol L⁻¹ solution containing 10⁻⁴ mol L⁻¹ of uranium. Based on this calculation the U(VI) over U(IV) ratio did not
177 exceed 1 mol. %. The calculations (see Figure S2 of the supporting data) indicated that the f(O₂) did not exceed 10⁻⁶⁹
178 atm. As stated by Rai et al. (1990), such a low value for the O₂(g) fugacity ensures that the uranium remains
179 tetravalent. This fugacity was then used in the calculation of the speciation of the dissolved uranium. For all
180 subsequent calculations, the ratio [UO₂²⁺]/[U] ≈ 1% was used.

181

182 3. RESULTS

183 3.1. Characteristics of the solids

184 PXRD patterns of synthesized and pure coffinite samples are shown in Figure 1. All of the samples were prepared
185 for 16 days at pH = 11.2 before the buffering step at T = 250°C. Three phases were identified: coffinite, nanoscale
186 crystals of UO₂ and amorphous SiO₂ (the latter being identified by SEM and X-EDS measurements). The specific
187 surface areas of the as-prepared sample and the pure coffinite were not significantly different and reached 38 ± 2 m²
188 g⁻¹. Additionally, the PXRD pattern of the sample obtained at pH = 12.5, before the buffering step, clearly shows the
189 presence of UO₂ nanoparticles as the only crystalline phase. For the refinement of the X-ray data, two phases were
190 considered: tetragonal USiO₄ (*I4₁/amd*): **a** = 6.9920(1) Å, **c** = 6.2633(1) Å and V = 306.20(1) Å³ and isometric UO₂
191 (*Fm $\bar{3}$ m*): **a** = 5.4329(1) Å and V = 160.36(1) Å³. The amount of USiO₄ vs. UO₂ was quantified based on PXRD data
192 from the Rietveld refinement (Table 2). The complete characterization of the synthesized solids has been reported by

193 Mesbah et al., (2015) in order to confirm that only U(IV) was present in the solids. In addition, EXAFS and Raman
194 spectroscopies were used to confirm that only U(IV)-based compounds were obtained from the synthesized and
195 purified powders, consistent with previous reports on coffinite (Clavier et al., 2014; Dreissig et al., 2011).

196 TEM images and associated electron diffraction patterns of a coffinite grain isolated in the pure coffinite sample
197 obtained after three purification cycles and one coffinite grain surrounded by uranium oxide nanoparticles in the as-
198 prepared sample are shown, in Figure 2 (a) and (b), respectively. These images show well crystallized coffinite grains,
199 200 to 400 nm. The crystallites (*i.e.*, the length of coherent domains determined by Rietveld refinement), which
200 formed the grains, were ~80 nm, confirming the polycrystalline nature of the coffinite grains. Grain size can affect the
201 thermodynamic properties of crystalline materials (Castro, 2013), the particle size of this synthetic sample is similar
202 to that of natural coffinite and that produced by the corrosion of spent nuclear fuel (Bros et al., 2003; Deditius et al.,
203 2012; Deditius et al., 2008; Janeczek, 1999; Janeczek and Ewing, 1992b; Jensen and Ewing, 2001; Pownceby and
204 Johnson, 2014); thus, the data obtained here are representative of the occurrence of coffinite in nature and as an
205 alteration product of UO₂ in spent nuclear fuel. The TEM images of the as-prepared samples also revealed the
206 presence of uranium oxide nanoparticles, 3 to 5 nm in diameter. The length of coherent domains determined by
207 Rietveld refinement for the UO₂ phase reached 4 nm. This analysis indicated that diffraction occurs from essentially
208 the entire particle. These structural observations are consistent with the structural model proposed by Schofield et al.
209 (2008) for biogenic uraninite nanoparticles of ~2 nm. They showed through synchrotron powder diffraction and
210 EXAFS, that UO₂ sublattice is preserved in the biogenic sample (as in our nanoparticles), and they assumed that
211 structural distortion is local, mostly occurring in the periphery of the particles. Another important result is that such
212 biogenic nanoparticles are structurally homologous to stoichiometric UO_{2.00}. One proposed explanation is that
213 hyperstoichiometric UO_{2+x} is stabilized by the presence of U(VI) impurities that are exsolved from the bulk UO₂ as a
214 nanoscale phase. Such phase segregation may not be possible in nanoparticles because they are too small. However,
215 we cannot exclude this possibility because the size of the nanoparticles in the as-prepared sample is slightly greater
216 than that of biogenic nanoparticles, and the mechanism of formation is not promoted by biogenic processes that could
217 prevent the incorporation of U(VI).

218 The average U/Si mole ratio determined by X-EDS corresponding to each sample is reported in Table 2. The
219 distributions of U/Si mole ratios for the as-prepared, purified and pure coffinite samples are shown in Figure 3 (a), (b)
220 and (c), respectively. The distribution of the U/Si mole ratios corresponding to the as-prepared sample was found to

221 be rather wide (with values ranging from 0.13 to 1.68), which reflects the presence of UO_2 and amorphous SiO_2 . The
222 composition of the mixture of three components was estimated by both XRD and EDS analysis. The molar ratios are:
223 59 mol. % of USiO_4 , 24 mol. % of UO_2 and 16 mol. % of amorphous SiO_2 . After three purification cycles (each
224 purification cycle consisted of the following steps: *i.*) the solid was placed in contact with HNO_3 then washed
225 with deionized water; *ii.*), the remaining solid was placed in contact with KOH and washed three times with deionized
226 water) the distribution of U/Si mole ratios was narrowed. After this treatment, the average U/Si mole ratio was $1.01 \pm$
227 0.08 , which is that of the pure coffinite. An SEM micrograph of the pure coffinite is shown in Figure 3 (c). For the
228 sample that underwent only two purification cycles, the distribution of the U/Si mole ratio, as determined by X-EDS,
229 shifted towards values lower than 1, indicating the presence of amorphous SiO_2 , also confirmed by SEM (Figure 3
230 (b)). Throughout the paper, the $\text{USiO}_4 + \text{SiO}_2$ assemblage obtained after two purification cycles is identified as a
231 “purified sample”. These observations clearly show that three purification cycles are required in order to remove the
232 entire amount of oxide by-products through dissolution and that the resulting sample was finally single-phase
233 coffinite.

234

235 3.2. Dissolution experiments

236 The evolution of elemental concentrations obtained during dissolution experiments at 298 K are presented in Figure
237 4. For the experiments completed under an Ar atmosphere, a plateau was reached within 30 to 50 days of leaching
238 time. Under these conditions, the system was considered to be at thermodynamic equilibrium when at least three
239 consecutive analyses were in the range of two standard deviations. The composition of the solution at saturation with
240 respect to the solid phase was then calculated as the average of consecutive analyses that were not significantly
241 different from each other. Finally, the average concentrations of the solutions at thermodynamic equilibrium with the
242 solids, as well as the average pH of each experiment, are given in Table 4. The error associated with elemental
243 concentrations and pH indicated in Table 4 represents the experimental error, as it resulted from the variability
244 observed between at least three consecutive analyses of the solution at steady-state.

245 All samples, except the pure coffinite exhibited nonstoichiometric dissolution. For example, dissolution tests of the
246 as-prepared sample showed a U/Si mole ratio of 5 during the first days of dissolution (Figure 4 (a)) that clearly
247 indicates the preferential dissolution of the UO_2 nanoparticles as compared with SiO_2 , and this was confirmed by the
248 evolution of U and Si concentrations for the $\text{UO}_2 + \text{SiO}_2$ assemblage (Figure 4 (d)). Under the experimental

249 conditions considered (0.1 mol·L⁻¹ HCl, Ar atmosphere), the dissolution of UO₂ nanoparticles was rapid and led to U
 250 concentration higher than 10⁻³ mol L⁻¹ in solution after only one day. However, after 60 days of leaching, the
 251 dissolution of the as-prepared sample became virtually stoichiometric (U/Si = 1.4). Then, the U and Si concentrations
 252 reached a constant value after almost 70 days. Importantly, the elemental concentrations obtained at steady-state for
 253 the as-prepared sample (UO₂ + SiO₂ + USiO₄) and the pure coffinite are very close. Consequently, we assume that the
 254 coffinite phase controlled this equilibrium. Thus, the solubility of the coffinite was reached from over-saturated
 255 conditions, whereas it was reached from under-saturated conditions for the pure coffinite solubility experiment
 256 (Figure 4 (b)). The purified sample (USiO₄ + SiO₂) exhibited a different trend than the as-prepared sample due to the
 257 absence of UO₂ nanoparticles (Figure 4 (c)). The U/Si molar ratio was lower than 1 for the entire duration of the
 258 experiment. The Si concentration increased during the first 30 days of dissolution, then reached a constant value.
 259 Simultaneously, the uranium concentration decreased and stabilized. Assuming that the coffinite phase controlled the
 260 equilibrium, the rapid dissolution of amorphous silica led to over-saturated conditions for USiO₄. In the case of the as-
 261 prepared sample, these oversaturation conditions were imposed by the faster dissolution of UO₂ nanoparticles.
 262 Oversaturation conditions were created by the faster dissolution of amorphous SiO₂ in the case of the purified sample.
 263 In both cases, the resulting uranium concentration decreased. A dissolution test of the UO₂+SiO₂ assemblage (Figure
 264 4 (d)) indicated an initial rapid dissolution of UO₂ nanoparticles and amorphous SiO₂ followed by a steady-state
 265 concentration. The solubility of amorphous SiO₂ was reached after 50 days based on the value provided by the
 266 thermochemie_PHREEQC_SIT_v9 database: (log *K_S^o(SiO₂,am) = -2.710). This could be the explanation for the
 267 constant silica concentration. The uranium concentration also stabilized at a value of 2.6 10⁻³ mol L⁻¹ after 50 days of
 268 dissolution, which was more than one order of magnitude higher than for the phases assemblages containing coffinite.
 269 This value corresponds to a solution oversaturated with respect to UO₂(cr), with a saturation index,
 270
$$SI = \log \left(\frac{\text{Ion activity product}}{K_S^o} \right)$$
, of about 4 (based on the NEA-TDB value for the solubility product), but
 271 undersaturated with respect to UO₂(am), with a saturation index of -2.4 (based on the NEA-TDB value for the
 272 solubility product). As previously stated in the review of Neck and Kim (2001), values reported in the literature for
 273 solubilities of UO₂·xH₂O(s) are extremely scattered. These discrepancies are ascribed either to different redox
 274 conditions or to different degrees of crystallinity (Casas et al., 1998; Rai et al., 1990). The uranium oxide phase in our
 275 samples cannot be described as amorphous, as the PXRD patterns showed broad diffraction maxima characteristic of

276 nanometric crystals. A possible effect of grain size on solubility was proposed by Casas et al. (1998) based on the
277 relation established by Stumm et al., (1992). Small crystals are thermodynamically less stable and have a greater
278 solubility than larger ones. This could possibly explain the high uranium concentration observed for the UO_2+SiO_2
279 mixture. More importantly, the role of silicates in this experiment is not taken into account in the evaluation of
280 tetravalent uranium speciation. The existence of U(IV)-Si(IV) complexes is undocumented, but they could play an
281 important role in coffinite formation (Mesbah et al., 2015). Due to similar charge and ionic radius, the analogy
282 between U(IV) and Th can be made. Peketroukhine et al. (2002) showed that the solubility of amorphous thorium
283 hydroxide was increased in the presence of soluble silicates in 0.1 M NaClO_4 and at pH 6-12. They reported a
284 solubility of 10^{-6} to 10^{-5} mol L^{-1} Th(IV) respectively at pH = 8 and 10 in the presence of 0.14 mol L^{-1} Na_2SiO_3 . This
285 increase was attributed to the formation of colloids of thorium hydroxo-silicate whose solubility was higher than that
286 of $\text{ThO}_2 \cdot n\text{H}_2\text{O}$. Rai et al. (2008), reported similar results. The interpretation of their data required the existence of a
287 mixed thorium hydroxo-silicate complex, $\text{Th}(\text{OH})_3(\text{H}_3\text{SiO}_4)_3^{2-}$ whose structure was determined by DFT calculations.
288 If the existence of such mono- or polynuclear complexes could be demonstrated for uranium, this would be a serious
289 limitation on the interpretation of uranium oxide solubility experiments performed without dissolved silicates.

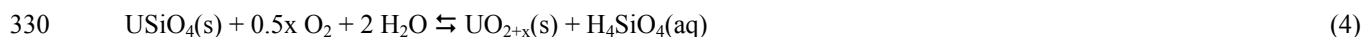
290 The dissolution experiments were also completed under air. Under these conditions, tetravalent uranium is usually
291 found to be unstable. Thus, the impact of oxygen partial pressure on the dissolution of coffinite was evaluated only
292 from a kinetic point of view by the comparison of the normalized dissolution rates obtained under the anoxic
293 condition with those obtained under air. The influence of oxygen partial pressure on the uranium chemistry at the
294 solid/liquid interface or in solution has extensively demonstrated during the dissolution or leaching of UO_2 . The
295 corrosion process of UO_2 in an oxic environment involves the complete conversion of tetravalent uranium into
296 hexavalent UO_2^{2+} and the formation of secondary phases (Baker, 2014; Maher et al., 2012). The rate of this alteration
297 process strongly depends on the activity of dissolved O_2 (Amme et al., 2005; Shilov et al., 2007); thus, on the partial
298 pressure of $\text{O}_2(\text{g})$. Jerden and Sinha (2003), studied the alteration of primary ore samples from Coles Hill deposit
299 (Virginia, USA) by oxygenated recharge water (from 4 to 8 mg L^{-1} dissolved O_2). The process by which uranium is
300 released from coffinite (most abundant U^{4+} mineral in the Coles Hill deposit) to groundwater through the oxidation
301 and dissolution of the primary minerals occurred within 4 to 5 weeks in highly fractured zones. However, the kinetics
302 of this process had never been studied using synthetic, pure coffinite.

303 The release of an element i from the material is usually described by its normalized mass loss, $N_L(i)$ (g m^{-2}) and by
304 the initial normalized dissolution rate $R_{L,0}(i)$ ($\text{g m}^{-2} \text{d}^{-1}$), calculated as follows:

$$305 \quad N_L(i) = \frac{\Delta m_i}{f_i S} = \frac{C_i V}{f_i S} \quad \text{and} \quad R_{L,0}(i) = \frac{dN_L(i)}{dt}, \quad (3)$$

306 where Δm_i (g) is the mass of element i released in solution; C_i (g L^{-1}) is the elementary concentration; V (L) is the
307 volume of the dissolution medium; S (m^2) is the surface area of the solid determined by the B.E.T. method and f_i
308 (dimensionless) is the mass fraction of i in the solid.

309 Thereafter, the dissolution reaction is considered to be congruent when all of the normalized dissolution rates are
310 identical (*i.e.* when all the elements were released with the same ratios as the stoichiometry of the initial material).
311 The initial normalized dissolution rates determined for the pure USiO_4 sample and the $\text{UO}_2 + \text{SiO}_2$ assemblage in out-
312 gassed 0.1 mol L^{-1} HCl solution, either under Ar atmosphere or in air, are summarized in Table 3. The dissolution of
313 USiO_4 was found to be congruent regardless of the dissolution conditions. The normalized dissolution rates of both U
314 and Si increased by one order of magnitude in HCl solution equilibrated with air (from $3 \cdot 10^{-5}$ to $3.8 \cdot 10^{-4} \text{ g m}^{-2} \text{d}^{-1}$) as
315 compared with the experiments performed under an argon atmosphere, while the normalized dissolution rates for UO_2
316 increased by a factor of almost 20 (from $6 \cdot 10^{-4}$ to $1.1 \cdot 10^{-2} \text{ g m}^{-2} \text{d}^{-1}$). On the contrary, and as expected, the kinetics of
317 SiO_2 dissolution was not significantly affected by the increase of $p\text{O}_2$ and $p\text{CO}_2$. To our knowledge, there is no
318 previous study of the kinetics of dissolution of synthetic coffinite. The dissolution rate of UO_2 nanoparticles in the
319 $\text{UO}_2 + \text{SiO}_2$ sample under reducing conditions can be compared with values obtained by Bruno et al. (1991) for $50 \mu\text{m}$
320 grains size $\text{UO}_{2,001}$ (exhibiting low specific surface area of $0.201 \text{ m}^2 \text{g}^{-1}$) and by Ulrich et al. (2008) for biogenic
321 nanoparticles of $\text{UO}_{2,00}$ (exhibiting a high specific surface area, $50.14 \text{ m}^2 \text{g}^{-1}$). Interestingly, the dissolution rates of
322 UO_2 at $\text{pH } 1$ under reducing conditions, calculated by using the rate laws provided either by Bruno et al. (1991) or
323 Ulrich et al. (2008) are close (0.08 and $0.4 \text{ g m}^{-2} \text{d}^{-1}$, respectively) and several orders of magnitude higher than the
324 value determined in our study ($6.0 \pm 0.8 \cdot 10^{-4} \text{ g m}^{-2} \text{d}^{-1}$). This decrease in the normalized dissolution rate indicates that
325 under reducing and acidic conditions, the amorphous SiO_2 in which UO_2 nanoparticles are embedded could act as a
326 passive layer, preventing protons access to the reactive surface sites. As noted by Amme et al. (2005), coffinite is
327 susceptible to release of uranium in oxygenated water in a manner similar to that of UO_2 . However, the normalized
328 dissolution rate of coffinite was at least one order of magnitude lower than that for UO_2 . As proposed by Janeczek and
329 Ewing (1992b), the replacement of coffinite by uraninite may be written as:



331 Following reaction (4), higher values of oxygen fugacity might favor the formation of non-stoichiometric uranium
 332 dioxide as an intermediate solid phase, which would be then dissolved after complete oxidation of U(IV) to U(VI).
 333 Thus, the steady-state concentration of uranium depends on the rate of formation of a partially oxidized UO_{2+x} from
 334 coffinite (following reaction 4) and the rate of dissolution of the intermediate UO_{2+x} .

335 The PXRD patterns of USiO_4 sample measured after dissolution either under Ar atmosphere or in air are shown in
 336 Figure 5. In both cases, the PXRD patterns exhibit the characteristic XRD diffraction maxima of coffinite with no
 337 evidence of additional secondary phases. Under these conditions, the solubility constant of USiO_4 was determined
 338 from the elemental concentrations measured in solution under Ar atmosphere and the pH at equilibrium that was
 339 found to range from 1.09 to 1.33 (Table 4).

340

341 4. DISCUSSION

342 4.1. Thermodynamic analysis

343 The determination of the solubility product is based on the data obtained for each system under steady-state
 344 conditions. Due to the oxidation of tetravalent uranium to hexavalent uranyl species during the dissolution, the results
 345 obtained in air were not considered in the thermodynamic analysis. For the oxygen-free experiments, the system was
 346 considered to be at thermodynamic equilibrium when at least three consecutive analyses were in the range of two
 347 standard deviations. The composition of the solution at saturation with respect to the solid phase was then calculated
 348 as the average of consecutive analyses that were not significantly different from one another. Finally, the average
 349 concentrations of the solutions at thermodynamic equilibrium with the solids, as well as the average pH values used in
 350 these calculations are compiled in Table 4. The errors associated with elemental concentrations and pH indicated in
 351 Table 4 represent the experimental error as calculated from the measured values among at least three consecutive
 352 analyses of the system at steady-state.

353 The thermodynamic equilibrium between coffinite and the solution is written following reaction (2). Thus, the
 354 solubility product of coffinite was calculated using the general equation:

355
$$*K_s^\circ(\text{USiO}_4) = (\text{U}^{4+})(\text{H}_4\text{SiO}_4)(\text{H}^+)^{-4} \quad (5)$$

356 where () denotes the activity of ions in solution at equilibrium.

357 The solubility product calculated at $I = 0$ can be deduced from the solubility product determined at $I = 0.1 \text{ mol L}^{-1}$
 358 following:

$$359 \quad {}^*K_S^\circ(\text{USiO}_4) = (\gamma_{\text{U}^{4+}} m_{\text{U}^{4+}}) (\gamma_{\text{H}_4\text{SiO}_4} m_{\text{H}_4\text{SiO}_4}) (\gamma_{\text{H}^+} m_{\text{H}^+})^{-4} = \prod_i (\gamma_i^{\nu_i}) {}^*K_S(\text{USiO}_4) \quad (6)$$

360 where γ_i denotes the activity coefficient for ion i , ν_i is the stoichiometric coefficient, and m_i (mol kg^{-1}) is the molality
 361 of i .

362 From the average elemental concentrations, pH value and the calculated oxygen fugacity $f(\text{O}_2)$ (10^{-69} atm), in the
 363 system at equilibrium, the molalities were calculated with the geochemical speciation model PHREEQC-2 (Parkhurst
 364 and Appelo, 1999). The solubility product calculations accounted for the aqueous complexation reactions listed in the
 365 Table 1. The ANDRA Thermochemie thermodynamic database, recently available for the PHREEQC software, was
 366 used. In the ANDRA Thermochemie database, the existence of $\text{U}(\text{OH})_2^{2+}$ and $\text{U}(\text{OH})_3^+$ and the associated equilibrium
 367 constants from Neck and Kim (2001) are taken into account. The values selected by the NEA-TDB (Grenthe et al.
 368 1992; Guillaumont et al., 2003) are systematically included in this database and recalculated for internal consistency.
 369 The values of the equilibrium constants and solubility products of the ANDRA Thermochemie database can be
 370 compared to other sources in Table 1. The speciation calculations indicate that the U^{4+} species represented 29 to 34
 371 mol. % of the tetravalent uranium under the experimental conditions, whereas $\text{U}(\text{OH})_2^{2+}$, $\text{U}(\text{OH})_3^+$, and UCl^{3+} species
 372 were in the same range, between 20 and 25 mol. %. UO_2^{2+} molality depended on the $f(\text{O}_2)$ selected and reached
 373 almost 1 mol. %. As the estimate of $m_{\text{U}^{4+}}$ was affected by the experimental uncertainty of pH, the speciation
 374 calculations were made at a maximum and a minimum pH value, defined as the average pH value ± 2 standard
 375 deviations in order to estimate a confidence interval for $m_{\text{U}^{4+}}$. The estimate of $m_{\text{H}_4\text{SiO}_4}$ was not affected by the
 376 uncertainty of the pH values, as H_4SiO_4 is the predominant species in this range of pH. The uncertainty in the
 377 evaluation of $m_{\text{H}_4\text{SiO}_4}$ thus depends only on the variability observed experimentally for the Si concentration at
 378 equilibrium between successive measurements. Finally, the uncertainty in the determination of *K_S was estimated by
 379 propagating the uncertainties on $m_{\text{U}^{4+}}$, $m_{\text{H}_4\text{SiO}_4}$, and m_{H^+} .

380 The activity corrections were performed using the specific ion interaction equation implemented in PHREEQC-2:

$$381 \quad \log(\gamma_i) = -\frac{A z_i^2 \sqrt{I_m}}{1 + B a_i \sqrt{I_m}} + \sum_j \varepsilon(i, j, I_m) m_j \quad (7)$$

382 where A and Ba_i are constants that depend on the temperature and are defined in the database (at 25°C and 1 bar, $A =$
 383 $0.509 \text{ kg}^{1/2} \text{ mol}^{-1/2}$, $Ba_i = 1.5 \text{ kg}^{1/2} \text{ mol}^{-1/2}$), z_i corresponds to the charge of the ion, I_m (mol kg^{-1}) is the ionic strength of
 384 the solution. The calculated activities of U^{4+} and H_4SiO_4 at equilibrium, as well as the solubility constant extrapolated
 385 to standard conditions, $*K_S^\circ$, are listed in Table 4.

386 The log $*K_S^\circ$ values obtained from the three phase assemblages that contained USiO_4 range from -4.63 to -5.34.
 387 The only value that was found to be significantly different from others was obtained for the phase assemblage USiO_4
 388 + SiO_2 #2 in Table 4. This difference resulted from a significantly higher pH value at equilibrium. As the presence of
 389 coffinite was not detected in the PXRD pattern of the $\text{UO}_2 + \text{SiO}_2$ assemblage at the end of the dissolution
 390 experiment, the value of $*K_S$ was not calculated. However, considering the values of the activities of U^{4+} and H_4SiO_4
 391 at steady state, supersaturated conditions should have been reached relative to coffinite. The value determined for the
 392 pure coffinite sample is: $\log *K_S^\circ(\text{USiO}_4, \text{cr}) = -5.25 \pm 0.05$. This value was selected afterwards as it corresponds to
 393 the pure coffinite sample, the solubility product can thus be attributed unambiguously to crystalline coffinite. This log
 394 $*K_S^\circ(\text{USiO}_4, \text{cr})$ value is higher than that estimated from solubility studies developed from uranotorite solid
 395 solutions: ($\log *K_S^\circ(\text{USiO}_4, \text{cr}) = -6.1 \pm 0.2$) (Szenknect et al., 2013). However, the thermodynamic calculations of
 396 that study were performed using the Lawrence Livermore National Laboratory (LLNL) database, whereas ANDRA
 397 Thermochemie database has been used in the present work. The main difference between the databases is the value of
 398 the equilibrium constant for the reaction: $\text{U}^{4+} + 4 \text{OH}^- \rightleftharpoons \text{U}(\text{OH})_4 (\text{aq})$, $\log K^\circ = 51.43$ for LLNL-TDB; whereas, it is
 399 46.0 in the ANDRA Thermochemie-TDB. This difference has a strong impact on the uranium speciation that led to a
 400 discrepancy of almost 1 log unit in the solubility product. Thus, it should be stressed here, that the choice of the
 401 thermodynamic database is a key step in the evaluation of standard equilibrium constant and that the estimate of error
 402 does not take into account the uncertainties on the thermodynamic constants implemented in the database. Thus, using
 403 the solubility product reported here for coffinite with a different set of thermodynamic data will lead to inconsistent
 404 and erroneous results.

405 The variation of the standard Gibbs energy associated with reaction (2) was then determined as:

$$406 \quad \Delta_r G^\circ(T) = -RT \ln *K_S^\circ(T) \quad (8)$$

407 where R is the universal gas constant and T is the absolute temperature.

408 The $\Delta_r G^\circ(298\text{ K})$ for reaction (2) determined in this study and the $\Delta_f G^\circ$ of the species involved in reaction (2) taken
409 from the NEA TDB II (Table S1 of the supporting information) were used in the Hess's law (Eq. 9) to determine the
410 standard molar Gibbs energy of formation of coffinite:

$$411 \quad \Delta_r G^\circ = \sum_i \nu_i \Delta_f G^\circ \quad (9)$$

412 The standard Gibbs energy of formation of coffinite from the elemental concentrations in solution was found to be:
413 $\Delta_f G^\circ(298\text{ K}) = -1867.6 \pm 3.2\text{ kJ mol}^{-1}$. As already mentioned, very few reliable thermodynamic data related to
414 coffinite formation or solubility are reported in the literature. Table 5 provides a comparison of the thermodynamic
415 data reported in this work to previously published data.

416 The relative stability of coffinite as compared with the binary mixture of the oxides can be derived from the
417 $\Delta_{r,ox} G^\circ(T)$ value associated with reaction (10)



419 The value of $\Delta_{r,ox} G^\circ(298\text{ K})$ was calculated using $\Delta_f G^\circ$ of coffinite determined in this study and those of uraninite and
420 quartz (Table S1 of the supporting information). The obtained positive value reached $20.6 \pm 5.2\text{ kJ mol}^{-1}$, which
421 indicates unambiguously that coffinite is less stable than a quartz + uraninite mixture at 298 K. This is in agreement
422 with Hemingway (1982), who pointed out that coffinite must be less stable than the mixture of binary oxides in light
423 of the natural occurrence of coffinite and the paragenetic sequence described by Cuney in 1978 (Cuney, 1978). The
424 thermal stability of coffinite is not well known. Fuchs and Hoekstra (1959) placed the upper limit of coffinite stability
425 as compared with uraninite and amorphous silica at 1273 K. On the basis of this observation, Hemingway (1982)
426 estimated the Gibbs free energy related to the formation of coffinite from oxides at 298.15 K, assuming that the
427 $\Delta_{r,ox} G^\circ$ value of reaction (10) is equal to zero at 1273 K and using the heat capacities of quartz and uraninite to
428 approximate the heat capacity of coffinite between 298 and 1273 K, as well as auxiliary thermochemical data from
429 Robie et al. (1979). However, neither the $\Delta_{r,ox} G^\circ(298\text{ K})$ value of Hemingway ($2.12 \pm 8.01\text{ kJ}\cdot\text{mol}^{-1}$) nor the value
430 selected in the NEA TDB ($4.52 \pm 6.01\text{ kJ}\cdot\text{mol}^{-1}$) were accurate enough to reach a conclusion regarding the relative
431 stability of coffinite as compared with the mixture of binary oxides. The low value of the $\Delta_{r,ox} G^\circ(298\text{ K})$ of the
432 coffinitization reaction indicates that, depending on the sign of the $\Delta_{r,ox} H^\circ$, this equilibrium might be easily reversed
433 to favor the formation of coffinite at higher temperatures and pressures. Recent results obtained by Guo et al. (2015)
434 from calorimetry in sodium molybdate and lead borate and using the same pure coffinite sample as in the present

435 study, report $\Delta_{r,ox}H^\circ$ of 25.6 ± 3.9 kJ mol⁻¹. The substantially positive $\Delta_{r,ox}H^\circ$ also explains why coffinite cannot be
436 formed directly from the mixture of the binary oxides and decomposes upon heating to a moderate temperature as
437 observed by Guo et al. (2015). Using the Gibbs-Helmholtz equation, the $\Delta_{r,ox}H^\circ$ measured by Guo et al. (2015) for the
438 same coffinite sample and the $\Delta_{r,ox}G^\circ$ (298 K) determined by the solubility measurements in the present study, we
439 derived the standard molar entropy of formation of coffinite from the mixture of the binary oxides. The $\Delta_{r,ox}S^\circ$ term at
440 room temperature is: 17 ± 31 J mol⁻¹ K⁻¹. The same method was used to determine the standard entropy of formation
441 of coffinite: $\Delta_f S^\circ = -344 \pm 25$ J mol⁻¹ K⁻¹. The standard molar entropy can be calculated using auxiliary data from
442 Table S1, $S_m^\circ = 136 \pm 25$ J mol⁻¹ K⁻¹.

443 This analysis shows that coffinite is thermodynamically metastable relative to quartz and uraninite at 25°C. It is
444 noteworthy that isostructural ThSiO₄, thorite behaves differently. Mazeina et al. (2005) determined a $\Delta_{r,ox}H^\circ$ value for
445 the formation of thorite from thorianite and quartz that is slightly lower than for coffinite: $\Delta_{r,ox}H^\circ(\text{ThSiO}_4, \text{thorite}) =$
446 19.4 ± 2.1 kJ mol⁻¹. On the other hand, thorite was found to be more stable in Gibbs energy at 25°C than the mixture
447 of quartz and thorianite by Szenknect et al. (2013) and Schuiling et al. (1976). They obtained $\Delta_{r,ox}G^\circ(\text{ThSiO}_4, \text{thorite})$
448 $= -19.0 \pm 5.5$ and -25.0 ± 5.0 kJ mol⁻¹, respectively. In order for compounds with a positive $\Delta_{r,ox}H^\circ$ to have negative
449 $\Delta_{r,ox}G^\circ$, the entropy term must be large enough to offset the enthalpy. Thus, coffinite cannot be formed from the
450 mixture of uraninite and quartz; whereas, thorite, which is entropy stabilized, can be formed from thorianite and
451 quartz.

452

453 4.2. Environmental implications

454 In uranium ores, coffinite is commonly coexists with uraninite. Thus, the geologic evidence seems to contradict
455 these experimental results that confirm that coffinite is metastable relative to uraninite plus quartz. The calculation
456 based on the Gibbs free energy of formation of coffinite determined by the solubility measurements and auxiliary data
457 (Table S1) gives the Gibbs free energy of the coffinitization reaction (1) to be: -2.3 ± 5.6 , which is essentially zero
458 within error. Even though coffinite is metastable at room temperature with respect to crystalline UO₂ and SiO₂,
459 coffinite can form from aqueous U(IV) in contact with silica-rich solutions. From the recent review by Evins and
460 Jensen (2012), it appears that it is not possible to constrain the conditions that favor the formation of coffinite based
461 on geological occurrences because temperature, pressure, pH and silica activity of the fluids are not known.
462 Mercadier et al. (2011) estimate that the temperature of the mineralizing fluids in the Athabasca basin deposits

463 (Canada), where uraninite and coffinite precipitated in the uranium front, were not higher than 50°C. Mesbah et al.
464 (2015) showed that, under appropriate conditions, small amounts of coffinite in a UO₂ plus SiO₂ (amorphous) mixture
465 can be obtained by hydrothermal treatment at 150°C. The low yield of coffinite at low temperatures may result from
466 slow kinetics of nucleation, but hydrothermal conditions would not be required to precipitate coffinite. Finally, the
467 values of the silica and tetravalent uranium activity seem to be the key parameters that facilitate the precipitation of
468 coffinite.

469 The solubility product of coffinite determined experimentally in this study was used in the
470 Thermochimie_PHREEQC_SIT_v9 database for geochemical simulations using PHREEQC-2 software. This allows
471 one to delineate the stability fields of UO₂ and USiO₄ at low temperature in terms of silica activity and pH. The
472 conditions that favor the formation of coffinite as compared with uraninite at pH = 6 under anoxic condition are
473 shown in Figure 6. Using the solubility constant of uraninite selected by the NEA TDB project ($\log K_{s,0}^{\circ}(\text{UO}_2,$
474 crystalline, 298.15 K) = -60.86 ± 0.36), it appears that a solution in equilibrium with uraninite becomes supersaturated
475 with respect to coffinite if the silica concentration exceeds 0.41 mol L⁻¹. Such high silica concentrations are unlikely
476 in natural systems. This limit is obviously determined by the choice of the solubility constant for UO₂ that controls the
477 U(OH)₄ concentration in solution. However, this has been intensely debated (Langmuir, 1997; Neck and Kim, 2001;
478 Rai et al., 1990, 2003). Based on the assumption that amorphous UO₂ ($K_{s,0}^{\circ}(\text{UO}_2, \text{am}, 298.15 \text{ K}) = -54.5 \pm 1.0$)
479 controls the U(OH)₄ concentration, the lower limit of the silica concentration necessary to precipitate coffinite is 1.8
480 10⁻⁷ mol L⁻¹. The value measured by Parks and Pohl (1988), which is generally accepted for the solubility of
481 crystalline uraninite, corresponds to a silica concentration in solution of 1.8 10⁻⁶ mol L⁻¹, which is in equilibrium with
482 coffinite.

483 White (1995) reported the aqueous concentration of H₄SiO₄ in soil solutions and observed that the upper limit
484 corresponds to the solubility of amorphous SiO₂ (5 10⁻³ mol L⁻¹), whereas the lowest values were below the solubility
485 of quartz (less than 10⁻⁴ mol L⁻¹). Most of the soil solution data fall within the kaolinite stability field (silica
486 concentrations between 6.6 10⁻⁵ and 5 10⁻³ mol L⁻¹). Kaolinite is the most commonly reported weathering product of
487 silicate rocks in soils. Silica concentrations in soil solutions are thus strongly affected by the precipitation of
488 secondary clay minerals, even though, in some cases, the soil solution approaches saturation with primary silicate
489 minerals such as K-feldspar. Appelo and Postma (1996) reported the normal ranges of dissolved silica concentrations
490 in uncontaminated fresh water to be between 7 10⁻⁵ and 10⁻³ mol L⁻¹ (gray area in Figure 6). Thus, the values

491 commonly encountered for the dissolved silica concentrations in soil solutions and groundwaters are much higher
492 than the calculated limit of coffinite formation, considering the Parks and Pohl values for the solubility of uraninite.
493 Thus coffinitization of tetravalent uranium oxide whose solubility is intermediate between uraninite ($\log K_{s,0}^{\circ}(\text{UO}_2,$
494 $\text{cr}) = -60.86$) and $\text{UO}_2(\text{am})$ ($\log K_{s,0}^{\circ}(\text{UO}_2, \text{am}) = -54.5$) is possible at 298 K for silica concentrations that are common
495 in natural groundwaters. Figure 7 shows the variation of the tetravalent uranium concentration in solution with an
496 aqueous Si concentration of $7 \cdot 10^{-5} \text{ mol.L}^{-1}$ in equilibrium with coffinite at 298 K, under anoxic conditions as a
497 function of pH. Based on these calculations, it appears that a solution that contains more than $10^{-11} \text{ mol L}^{-1}$ of $\text{U}(\text{OH})_4$
498 is oversaturated with respect to coffinite in a pH range from 4 to 10. As this pH interval encompasses the typical
499 values for groundwater, the presence of coffinite in ores cannot be related to a precise range of pH that allows its
500 formation. However, it is important to stress that this solution remains oversaturated relative to uraninite. Elevated
501 silica and uranium concentrations are common in uranium ores, especially in sandstone deposits or highly
502 fractionated Si-rich igneous rocks (Amme et al., 2005; [Deditius et al., 2008](#); [Pownceby and Johnson, 2014](#); [Stieff et](#)
503 [al., 1955, 1956](#)). Different mechanism can lead to conditions oversaturated with respect to $\text{UO}_2(\text{s})$. For example, high
504 temperature brines can cause the dissolution of $\text{UO}_2(\text{crystalline})$ under reducing conditions, or U(IV) concentration
505 can increase in a redox front by reduction of U(VI). A high oversaturation is necessary to form $\text{UO}_2(\text{s})$ nuclei, and the
506 resulting U(IV) concentration may be orders of magnitude higher than the solubility of $\text{UO}_2(\text{cr})$. The degree of
507 crystallinity of uranium dioxide is another parameters that can affect its solubility. For natural UO_2 , it is strongly
508 affected by radiation damage. Small, metamict crystals are thermodynamically less stable; their dissolution in
509 appropriate conditions can lead to uranium concentration sufficiently high to form coffinite (Matzke, 1992). Most
510 importantly, the impact of silica in solution is not taken into account in the evaluation of tetravalent uranium
511 speciation; as a result, the evaluation of UO_2 solubility in silica-rich groundwater based on the currently available
512 thermodynamic data may not be correct. The existence of U(IV)-Si(IV) complexes is speculative, but Mesbah et al.
513 (2015) suggested that these complexes could play an important role in coffinite formation. The existence of mono- or
514 poly-nuclear complexes of U(IV) with silicates and hydroxydes, as it was evidenced for Th by Peketroukhine et al.
515 (2002) and Rai et al. (2008), would significantly increase the solubility of UO_2 under alkaline conditions and favor
516 coffinite precipitation. Such mechanism could explain the fact that uraninite and coffinite are often found in intimate
517 intergrowths in many natural samples (Deditius et al., 2008).

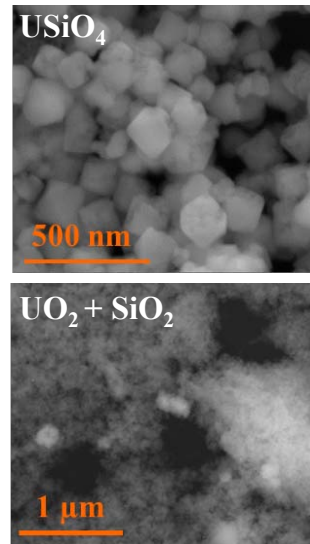
518 These results allow the assessment of the risk of coffinitization of UO_2 in the spent nuclear fuel in a geological
519 repository. Based on the values of the Si concentration ($1.4 \cdot 10^{-4} \text{ mol L}^{-1}$) measured by Gaucher et al. (2009) in the
520 French site porewater (Callovo-Oxfordian argillite), or in the granitic groundwater of Forsmark and Äspö in Sweden
521 ($1.8 \cdot 10^{-4} \text{ mol L}^{-1}$ and $1.5 \cdot 10^{-4} \text{ mol L}^{-1}$, respectively), it appears that coffinitization of the UO_2 matrix may occur only if
522 the dissolution of UO_2 matrix leads to tetravalent uranium concentrations in solution of at least $8 \cdot 10^{-12} \text{ mol L}^{-1}$.
523 Obviously, the concentration levels of U (IV) in the vicinity of the geological repository are hardly predictable.
524 Indeed, they are controlled by the dissolution rate of the UO_2 matrix in spent nuclear fuel, and this depends on the
525 groundwater velocity, composition (modified locally by radiolysis), pH, Eh and temperature, as well as the complex
526 microstructure and composition of the SNF (Burns et al., 2012). These parameters, which are spatially and temporally
527 variable (Ewing, 2015), in turn depend on the emplacement strategy and the types of near-field engineered barriers.

528

529 5. CONCLUSION

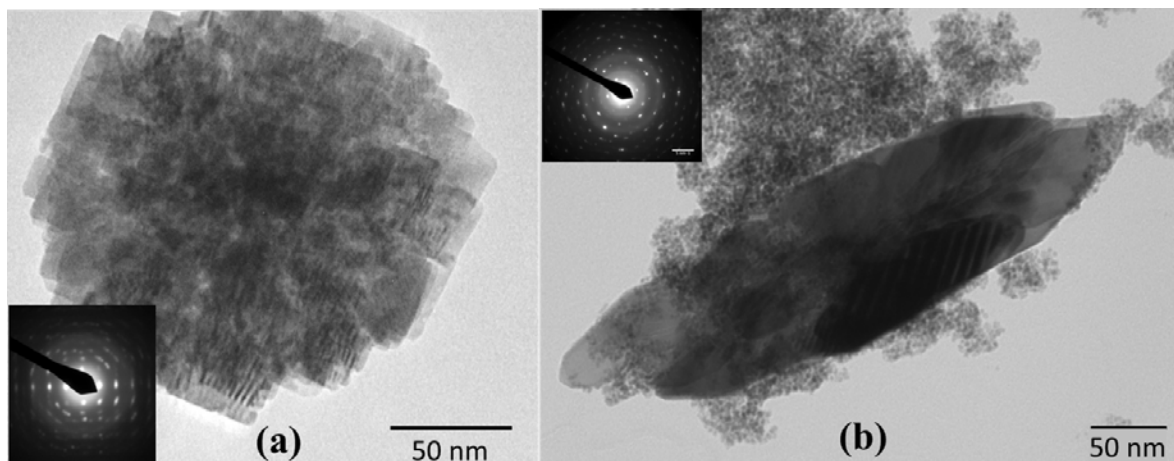
530 In response to the pressing need for more accurate thermodynamic data required for the evaluation of the formation
531 of coffinite, as well as the coffinitization of uraninite, the solubility constant of coffinite has been determined at 25°C
532 and 1 bar: $\log *K_S^\circ(\text{USiO}_4, \text{cr}) = -5.25 \pm 0.05$. This value, the first to be experimentally determined, allows for an
533 evaluation of the conditions under which the coffinitization of UO_2 may occur as a function of the pH and Si
534 concentration of the groundwater. Thermodynamically, the coffinitization reaction occurs at 298 K, under reducing
535 conditions, at near-neutral pH, for $[\text{U}(\text{OH})_4] \sim 10^{-11} \text{ mol L}^{-1}$ and $[\text{H}_4\text{SiO}_4] \sim 10^{-4} \text{ mol L}^{-1}$. Such silica and uranium
536 concentrations are common in uranium ores, especially in sandstone deposits or highly fractionated Si-rich igneous
537 rocks. This is consistent with the natural occurrence of coffinite. The positive value obtained for the $\Delta_{r,ox}G^\circ(298\text{K}) =$
538 $20.6 \pm 5.2 \text{ kJ mol}^{-1}$ associated with the formation of coffinite from a mixture of the binary oxides indicates that
539 coffinite is energetically metastable at low temperature with respect to uraninite plus quartz. Coffinite is thus formed
540 through a precipitation mechanism following the dissolution of uraninite in silica-rich solutions. Chemical
541 simulations indicate that coffinite is stable with respect to aqueous species over a wide range of concentrations, which
542 explains the occurrence of coffinite in uranium ore deposits. Although metastable with respect to uraninite and quartz,
543 coffinite persists in uranium ore deposits owing to its slow kinetics of dissolution.

544

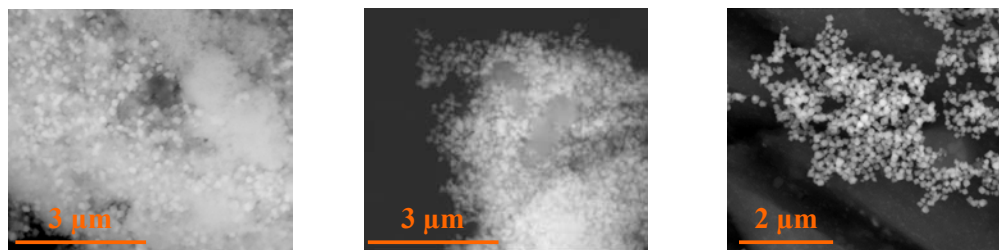


545
 546 Figure 1. PXRD patterns of an as-prepared sample obtained from the synthesis at pH =12.5 (black line), as-prepared
 547 sample obtained from the synthesis at pH = 11.4 (red line) and of the pure coffinite obtained after three purification
 548 cycles with HNO_3 10^{-2} mol L^{-1} and KOH 10^{-2} mol L^{-1} (blue line). SEM micrographs of the $\text{UO}_2 + \text{SiO}_2$ assemblage
 549 and of the pure coffinite sample.

550



551
 552 Figure 2. TEM images of (a) one grain of pure coffinite isolated in the sample obtained after three purification cycles
 553 and (b) one grain of coffinite surrounded by nanoparticles of uranium oxide by-product in the as-prepared sample.



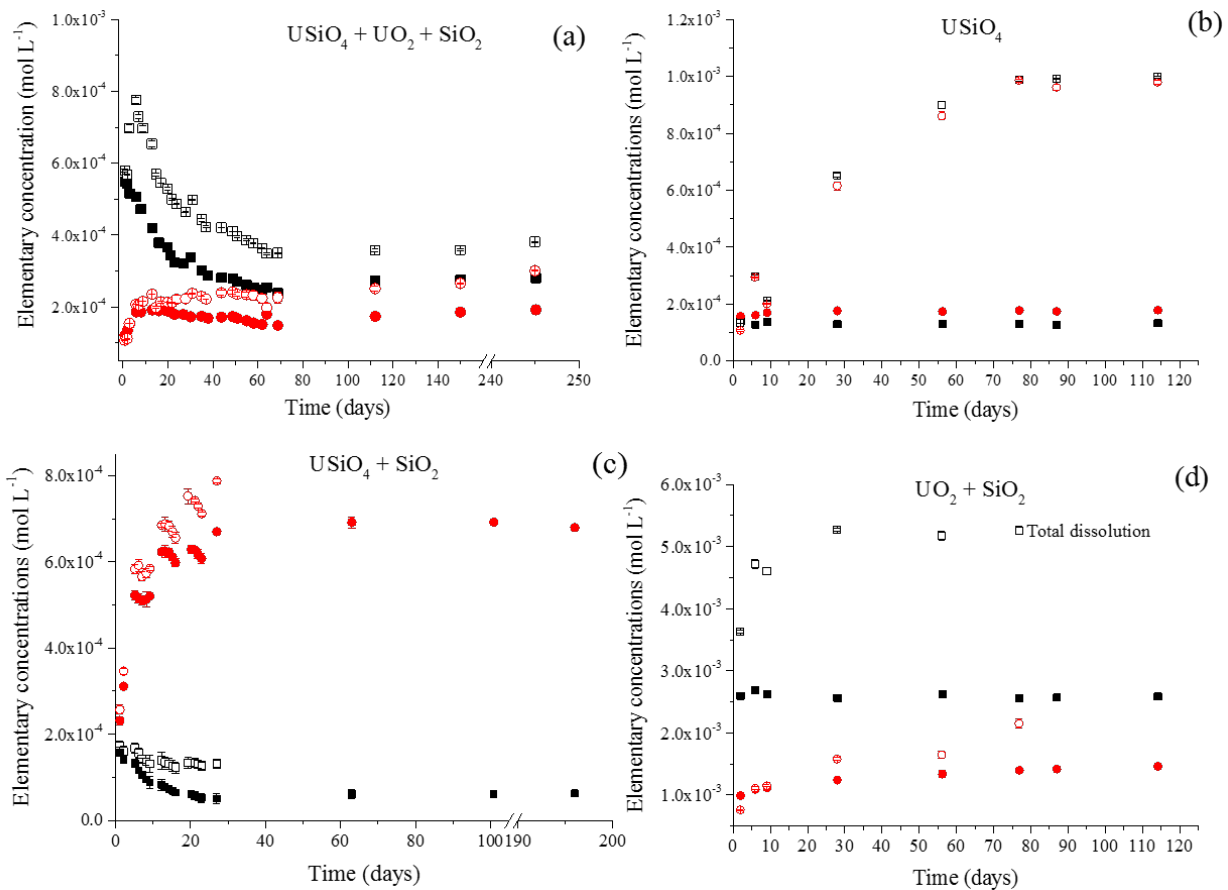
(a)

(b)

(c)

554
555
556 Figure 3. SEM micrographs and X-EDS analyses of (a) as-prepared sample, (b) sample after two purification cycles
557 with HNO_3 10^{-2} and KOH 10^{-2} mol L^{-1} and (c) pure coffinite sample obtained after three purification cycles.
558 Histograms represent the distribution of U/Si mole ratio determined by X-EDS (expressed in %).

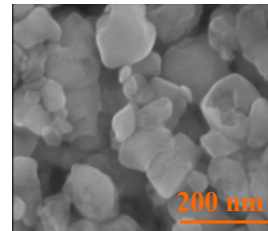
559



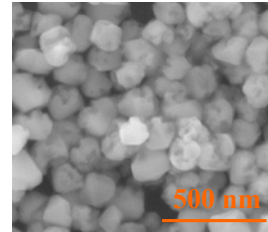
560
 561 Figure 4. Evolution of the elemental concentrations (U: black symbols, Si: red symbols) during the dissolution of (a)
 562 as-prepared sample containing USiO₄, UO₂ and SiO₂(am), (b) pure USiO₄, (c) purified sample containing USiO₄ and
 563 SiO₂(am) and (d) as-prepared containing UO₂ and SiO₂(am) only. Closed and open symbols are for experiments under
 564 an Ar atmosphere and air, respectively.

565

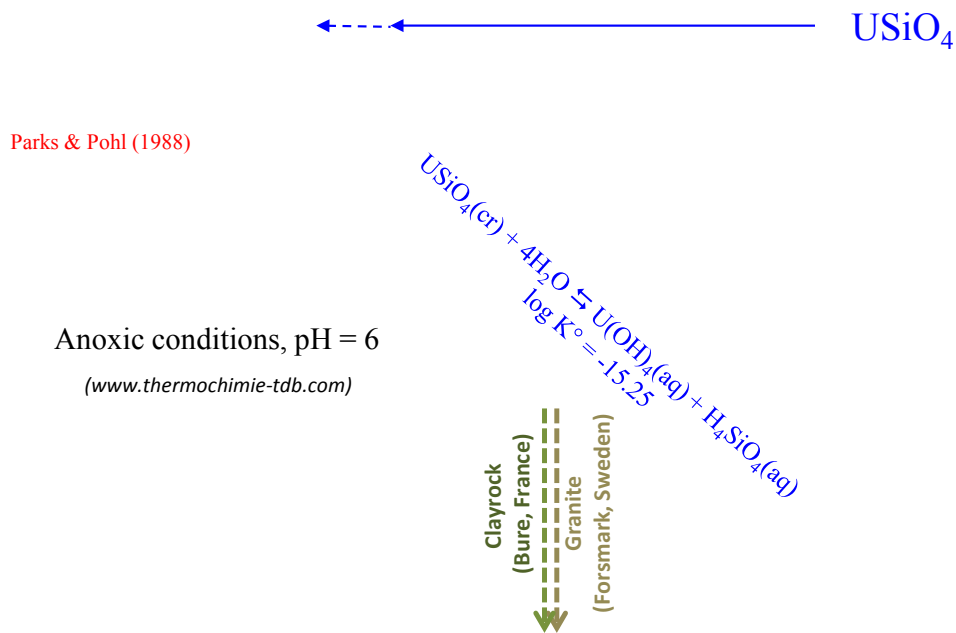
USiO₄ / Air



USiO₄ / Ar



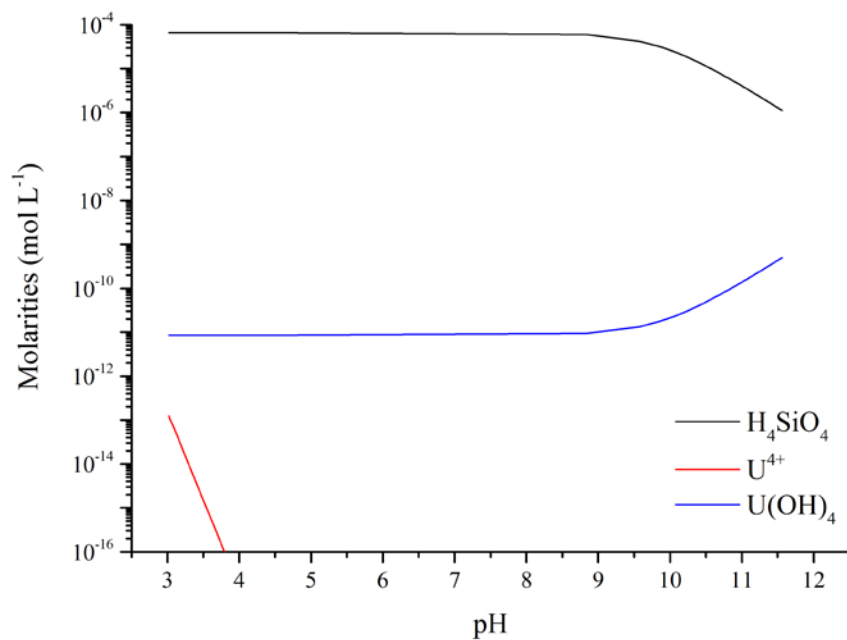
566
567 Figure 5. SEM images and PXRD patterns of USiO₄ sample at the end of under-saturated experiments performed in
568 0.1 M HCl solution under Ar atmosphere (black line) and under air (red line). Blue lines represent Bragg peak
569 positions for coffinite from JCPDS file #11-0420.



570

571 Figure 6. Plot of the tetravalent U concentration as a function of H₄SiO₄ concentration with the stability fields of
 572 coffinite. The diagram is constructed for pH = 6, f(O₂) = 10⁻⁶⁹ atm and Cl⁻ molarity of 0.01 mol L⁻¹, with log
 573 *K_s[°](USiO₄, cr) = - 5.25 ± 0.05. Dashed green line represents the lowest limit of the stability domain of coffinite for
 574 a silica concentration of 1.8 10⁻⁷ mol L⁻¹ assuming that the U(OH)₄(aq) concentration is controlled by the solubility of
 575 UO₂(am) (dashed green line). Solid green line represents the lowest limit of the stability domain of coffinite for a
 576 silica concentration of 0.41 mol L⁻¹ assuming that U(OH)₄(aq) concentration is controlled by the solubility of UO₂(cr)
 577 taken from NEA TDB (solid red line); dash-dot green line represents the lowest limit of the stability field for a silica
 578 concentration of 1.8 10⁻⁶ mol L⁻¹ assuming that the U(OH)₄(aq) concentration is controlled by the solubility of
 579 UO₂(cr) taken from Parks and Pohl (1988) (dash-dot red line). The gray area outlines the range of silica concentration
 580 encountered in soil solutions as reported by White (1995). The black square corresponds to the U(OH)₄(aq) and silica
 581 concentrations in the experiments performed by Amme et al. (2005).

582



583
 584 Figure 7. Variation of the $U(OH)_4$ concentration in equilibrium with coffinite (blue line) with the pH of the solution.
 585 Simulation was performed at 298 K for a total concentration of Si = $7 \cdot 10^{-5}$ mol L⁻¹ (corresponding to the left-hand
 586 limit of the gray area in figure 6), $f(O_2) = 10^{-69}$ atm, and ionic strength < 0.01 mol L⁻¹.

587
 588

589 Table 1. Thermodynamic data for the main reactions involving U and Si in the considered system extracted from the
590 Thermochemie_PHREEQC_SIT_v9 database (Giffaut et al., 2014) used in the thermodynamic calculations performed
591 to derive the solubility product of coffinite. The thermodynamic constants for the reactions involving U^{4+} included in
592 the Thermochemie-TDB were taken either from NEA thermodynamic database (Guillaumont et al., 2003) or from
593 Neck and Kim (2001) and recalculated for the internal consistency of the Thermochemie-TDB. The constant for the
594 formation of $Si_4O_6(OH)_6^{2-}$ was taken from Felmy et al. (2001), the solubility constant for $SiO_2(am)$ was taken from
595 Gunnarsson and Arnorsson (2000). The uncertainties associated with the selected values are reported only in the
596 original data sources.

Reaction	$\log K^\circ$	$\log K^\circ$	$\log K^\circ$
	Thermochemie-TDB	NEA-TDB	Neck and Kim, (2001)
$4 H^+ + 2 e^- + UO_2^{2+} = U^{4+} + 2 H_2O(l)$	9.04	9.038 ± 0.041	
$Cl^- + U^{4+} = UCl^{3+}$	1.72	1.72 ± 0.13	
$H_2O(l) + U^{4+} = H^+ + UOH^{3+}$	-0.54	-0.54 ± 0.06	-0.4 ± 0.2
$4 OH^- + U^{4+} = U(OH)_4(aq)$	46.0	46.0 ± 1.4	46.0 ± 1.4
$U^{4+} + 2 H_2O(l) = U(OH)_2^{2+} + 2 H^+$	-1.1		-1.1 ± 1.0
$U^{4+} + 3 H_2O(l) = U(OH)_3^+ + 3 H^+$	-4.7		-4.7 ± 1.0
$U^{4+} + 4OH^- = 2H_2O(l) + UO_2(am, hyd)$	54.5	54.5 ± 1.0	54.5 ± 1.0
$U^{4+} + 4OH^- = 2H_2O(l) + UO_2(cr)$	60.85	60.86 ± 0.36	60.86 ± 0.36
$Si(OH)_4(aq) = 2 H^+ + SiO_2(OH)_2^{2-}$	-23.14	-23.14 ± 0.09	
$Si(OH)_4(aq) = H^+ + SiO_2(OH)_3^-$	-9.84	-9.81 ± 0.02	
$4 Si(OH)_4(aq) = 4 H^+ + Si_4O_8(OH)_4^{4-} + 4 H_2O(l)$	-35.94	-36.3 ± 0.5	
$4 Si(OH)_4(aq) = 3 H^+ + Si_4O_7(OH)_5^{3-} + 4 H_2O(l)$	-25.10	-25.5 ± 0.3	
$4 Si(OH)_4(aq) = 2 H^+ + Si_4O_6(OH)_6^{2-} + 4 H_2O(l)$	-15.60		
$2 Si(OH)_4(aq) = 2 H^+ + Si_2O_3(OH)_4^{2-} + H_2O(l)$	-19.40	-19.0 ± 0.3	
$2 Si(OH)_4(aq) = H^+ + Si_2O_2(OH)_5^- + H_2O(l)$	-8.50	-8.1 ± 0.3	
$3 Si(OH)_4(aq) = 3 H^+ + Si_3O_6(OH)_3^{3-} + 3 H_2O(l)$	-29.30	-28.6 ± 0.3	
$3 Si(OH)_4(aq) = 3 H^+ + Si_3O_5(OH)_5^{3-} + 2 H_2O(l)$	-29.40	-27.5 ± 0.3	
$2 H_2O(l) + SiO_2(quar) = Si(OH)_4(aq)$	-3.74	-4.0 ± 0.1	
$2 H_2O(l) + SiO_2(am) = Si(OH)_4(aq)$	-2.71		

597

598 Table 2. Estimated quantities of USiO₄ and UO₂ based on Rietveld refinements of the PXRD patterns of the samples
 599 used for dissolution experiments and the corresponding cell parameters. Average U/Si molar ratio and two standard
 600 deviations determined from X-EDS analyses.

Sample ID	U/Si		USiO ₄				UO ₂			
	Mole ratio	a (Å)	c (Å)	Volume ^a (Å ³)	USiO ₄ (mol.%)	Crystal size (nm)	a (Å)	Volume (Å ³)	UO ₂ (mol.%)	Crystal size(nm)
USiO ₄ +UO ₂ +SiO ₂	1.14 ± 0.40	6.9879(1)	6.2614(1)	305.75(1)	61.0(3)	79(7)	5.4317(2)	160.26(1)	39.0(3)	4(1)
UO ₂ + SiO ₂	-	-	-	-	-	-	5.4180(4)	159.05(2)	100	4(1)
USiO ₄ +SiO ₂	0.65 ± 0.08	6.9833(2)	6.2575(2)	305.16(2)	100	79(7)	-	-	-	-
USiO ₄	1.01 ± 0.08	6.9856(2)	6.2582(2)	305.39(2)	100	79(7)	-	-	-	-

601 ^a the molar volume of USiO₄ reached V^o(298.15K) = 45.98 ± 0.04 cm³ mol⁻¹

602

603

604 Table 3. Initial normalized dissolution rates of USiO₄ and UO₂+SiO₂ samples determined in 0.1 mol L⁻¹ HCl at room
 605 temperature under Ar atmosphere and air, respectively.

Sample ID	Ar		Air	
	R _{L,0} (U) (g m ⁻² d ⁻¹)	R _{L,0} (Si) (g m ⁻² d ⁻¹)	R _{L,0} (U) (g m ⁻² d ⁻¹)	R _{L,0} (Si) (g m ⁻² d ⁻¹)
USiO ₄	(3 ± 2) 10 ⁻⁵	(6.0 ± 0.9) 10 ⁻⁵	(4.0 ± 0.2) 10 ⁻⁴	(3.8 ± 0.1) 10 ⁻⁴
UO ₂ + SiO ₂	(6.0 ± 0.8) 10 ⁻⁴	(2.1 ± 0.1) 10 ⁻⁴	(1.1 ± 0.2) 10 ⁻²	(1.5 ± 0.4) 10 ⁻⁴

606

607

608 Table 4. Composition of the equilibrated solutions from the dissolution experiments completed under Ar atmosphere
609 (calculated $f(\text{O}_2) = 10^{-69}$ atm) at 298 K in 0.1 mol L⁻¹ HCl. Elemental concentrations, [U] and [Si], are expressed in
610 mol L⁻¹. The calculated molalities of species are expressed in mol kg⁻¹. $*K_S(\text{USiO}_4)$ is the solubility product of USiO₄
611 for I = 0.1 mol L⁻¹. Activities of species in solution are calculated with the SIT equation. $*K_S^\circ(\text{USiO}_4)$ is the solubility
612 product of USiO₄ extrapolated to I = 0. $\Delta_r G^\circ$, $\Delta_f G^\circ$ and $\Delta_{r,ox} G^\circ$ are expressed in kJ mol⁻¹.

Sample ID:	USiO ₄	UO ₂ + SiO ₂ +USiO ₄		SiO ₂ +USiO ₄		UO ₂ + SiO ₂	
		1	2	1	2	1	2
[U]	(1.30 ± 0.04) 10 ⁻⁴	(2.63 ± 0.08) 10 ⁻⁴	(1.4 ± 0.2) 10 ⁻⁴	(5.7 ± 0.4) 10 ⁻⁵	(6.4 ± 0.3) 10 ⁻⁵	(2.58 ± 0.05) 10 ⁻³	(2.61 ± 0.05) 10 ⁻³
[Si]	(1.76 ± 0.07) 10 ⁻⁴	(1.7 ± 0.1) 10 ⁻⁴	(1.12 ± 0.07) 10 ⁻⁴	(6.3 ± 0.2) 10 ⁻⁴	(3.7 ± 0.1) 10 ⁻⁴	(1.63 ± 0.08) 10 ⁻³	(1.4 ± 0.1) 10 ⁻³
U:Si	0.74 ± 0.07	1.5 ± 0.1	1.3 ± 0.2	0.09 ± 0.01	0.17 ± 0.01	1.58 ± 0.11	1.9 ± 0.1
pH	1.15 ± 0.02	1.09 ± 0.02	1.17 ± 0.02	1.11 ± 0.02	1.33 ± 0.02	1.30 ± 0.02	1.30 ± 0.02
m_{H^+}	(8.8 ± 0.2) 10 ⁻²	(1.02 ± 0.02) 10 ⁻¹	(8.4 ± 0.2) 10 ⁻²	(9.7 ± 0.2) 10 ⁻²	(5.7 ± 0.1) 10 ⁻²	(6.2 ± 0.1) 10 ⁻²	(6.2 ± 0.1) 10 ⁻²
$m_{\text{U}^{4+}}$	(3.8 ± 0.1) 10 ⁻⁵	(8.8 ± 0.5) 10 ⁻⁵	(3.9 ± 0.5) 10 ⁻⁵	(1.8 ± 0.1) 10 ⁻⁵	(1.15 ± 0.08) 10 ⁻⁵	(5.5 ± 0.4) 10 ⁻⁴	(5.6 ± 0.4) 10 ⁻⁴
$m_{\text{UOH}^{3+}}$	(2.85 ± 0.09) 10 ⁻⁵	(5.5 ± 0.4) 10 ⁻⁵	(3.1 ± 0.4) 10 ⁻⁵	(1.2 ± 0.1) 10 ⁻⁵	(1.44 ± 0.07) 10 ⁻⁵	(5.9 ± 0.4) 10 ⁻⁴	(5.9 ± 0.4) 10 ⁻⁴
$m_{\text{U(OH)}_2^{2+}}$	(3.3 ± 0.2) 10 ⁻⁵	(5.3 ± 0.5) 10 ⁻⁵	(3.8 ± 0.5) 10 ⁻⁵	(1.3 ± 0.1) 10 ⁻⁵	(2.7 ± 0.1) 10 ⁻⁵	(9.7 ± 0.4) 10 ⁻⁴	(9.8 ± 0.4) 10 ⁻⁴
$m_{\text{U(OH)}_3^+}$	(5.6 ± 0.7) 10 ⁻⁸	(7.7 ± 0.9) 10 ⁻⁸	(6.8 ± 0.9) 10 ⁻⁸	(1.9 ± 0.2) 10 ⁻⁸	(7.3 ± 0.6) 10 ⁻⁸	(2.4 ± 0.2) 10 ⁻⁶	(2.4 ± 0.2) 10 ⁻⁶
$m_{\text{UCl}^{3+}}$	(3.0 ± 0.1) 10 ⁻⁵	(6.6 ± 0.4) 10 ⁻⁵	(3.1 ± 0.4) 10 ⁻⁵	(1.4 ± 0.1) 10 ⁻⁵	(1.02 ± 0.06) 10 ⁻⁵	(4.4 ± 0.2) 10 ⁻⁴	(1.02 ± 0.06) 10 ⁻⁵
$m_{\text{U(OH)}_4}$	(3.1 ± 0.5) 10 ⁻¹²	(3.7 ± 0.6) 10 ⁻¹²	(4.0 ± 0.5) 10 ⁻¹²	(1.0 ± 0.1) 10 ⁻¹²	(6.3 ± 0.9) 10 ⁻¹²	(1.9 ± 0.3) 10 ⁻¹⁰	(1.9 ± 0.3) 10 ⁻¹⁰
$m_{\text{UO}_2^{2+}}$	(1.21 ± 0.08) 10 ⁻⁶	(1.9 ± 0.9) 10 ⁻⁶	(1.4 ± 0.2) 10 ⁻⁶	(0.5 ± 0.2) 10 ⁻⁶	(1.0 ± 0.5) 10 ⁻⁶	(3.6 ± 1.9) 10 ⁻⁵	(3.6 ± 1.9) 10 ⁻⁵
$m_{\text{H}_4(\text{SiO})_4}$	(1.78 ± 0.07) 10 ⁻⁴	(1.7 ± 0.1) 10 ⁻⁴	(1.13 ± 0.07) 10 ⁻⁴	(6.4 ± 0.2) 10 ⁻⁴	(3.7 ± 0.1) 10 ⁻⁴	(1.64 ± 0.08) 10 ⁻³	(1.4 ± 0.1) 10 ⁻³
$*K_S(\text{USiO}_4)$	(1.1 ± 0.1) 10 ⁻⁴	(1.4 ± 0.1) 10 ⁻⁴	(0.9 ± 0.3) 10 ⁻⁴	(1.3 ± 0.2) 10 ⁻⁴	(4.0 ± 0.6) 10 ⁻⁵		
$\log *K_S(\text{USiO}_4)$	-3.95 ± 0.05	-3.86 ± 0.08	-4.05 ± 0.13	-3.88 ± 0.07	-3.40 ± 0.07		
(U ⁴⁺)	(7.9 ± 0.7) 10 ⁻⁷	(1.6 ± 0.7) 10 ⁻⁶	(8.4 ± 1.2) 10 ⁻⁷	(3.6 ± 0.3) 10 ⁻⁷	(3.0 ± 0.2) 10 ⁻⁷	(1.19 ± 0.08) 10 ⁻⁵	(1.20 ± 0.08) 10 ⁻⁵
(H ₄ SiO ₄)	(1.78 ± 0.07) 10 ⁻⁴	(1.7 ± 0.1) 10 ⁻⁴	(1.13 ± 0.07) 10 ⁻⁴	(6.4 ± 0.2) 10 ⁻⁴	(3.7 ± 0.1) 10 ⁻⁴	(1.64 ± 0.08) 10 ⁻³	(1.4 ± 0.1) 10 ⁻³
$*K_S^\circ(\text{USiO}_4)$	(5.6 ± 0.7) 10 ⁻⁶	(6.4 ± 1.1) 10 ⁻⁶	(4.5 ± 1.4) 10 ⁻⁶	(6.3 ± 1.0) 10 ⁻⁶	(2.4 ± 0.4) 10 ⁻⁵		
$\log *K_S^\circ(\text{USiO}_4)$	-5.25 ± 0.05*	-5.19 ± 0.08	-5.34 ± 0.13	-5.20 ± 0.07	-4.63 ± 0.07		
$\Delta_r G^\circ$	30.0 ± 0.3	29.6 ± 0.4	30.5 ± 0.8	29.7 ± 0.4	26.4 ± 0.4		
$\Delta_f G^\circ$	-1867.6 ± 3.2	-1867.2 ± 3.4	-1868.1 ± 3.7	-1867.3 ± 3.3	-1864.0 ± 3.3		
$\Delta_{r,ox} G^\circ$	20.6 ± 5.2	20.9 ± 5.4	20.0 ± 5.7	20.8 ± 5.3	24.1 ± 5.3		

613 *Value selected in the present study

614

615 Table 5. Review of the previous determinations of thermodynamic data for coffinite. Bold characters indicate the
616 values reported in publications (either estimated or measured). The other values were calculated in this study using
617 the reported ones (bold characters) associated with auxiliary data (see the footnotes for the source of auxiliary data),
618 or calculated using the Gibbs-Helmholtz equation.

	$\Delta_f G^\circ$	$\Delta_f H^\circ$	S_m°	$\Delta_f S^\circ$	$\Delta_{r,ox} G^\circ$	$\Delta_{r,ox} H^\circ$	$\Delta_{r,ox} S^\circ$	$\Delta_r G^\circ$	$\log {}^*K_S^\circ$
	kJ mol⁻¹	kJ mol⁻¹	J mol⁻¹ K⁻¹	J mol⁻¹ K⁻¹	kJ mol⁻¹	kJ mol⁻¹	J mol⁻¹ K⁻¹	kJ mol⁻¹	
Langmuir (1978)	-1891.17	-2001.21	117.15	-369.26 ¹	-3.10 ^a	-4.4 ^a	-1.3 ¹	52.38 ^a	-9.18
Langmuir & Chatham (1980)	-1882.38	-1990.33	117.15	-362.24 ¹	5.69 ^a	5.3 ^a	-1.4 ¹	43.60 ^b	-7.64
Hemingway (1982)	-1886 ± 20				2 ± 22 ^b			47 ± 23 ^b	-8 ± 4
Fleche (2002)	-1915.9 ± 32.4 ¹	-2021.7 ± 30.3	124.3 ± 6.6	-355.0 ± 7.0 ^c	-27.8 ± 34.4 ^c	-26.0 ± 32.3 ^c	6.0 ± 7.0 ¹	78.3 ± 35.3 ^c	-13.73 ± 6.19
Grenthe et al. (1992) Guillaumont et al. (2003)	-1883.6 ± 4.0	-1991.326 ± 5.367¹	118 ± 12	-361 ± 12 ^c	4.52 ± 6.06 ^c	4.374 ± 7.367 ^c	-0.49 ± 12.40 ¹	46.005 ± 6.921 ^c	-8.06 ± 1.21
Szenknect et al. (2013)	-1872.6 ± 3.8^c	-1980.3 ± 7.4 ¹	118 ± 12	-361 ± 12 ^c	15.5 ± 5.8^c	15.4 ± 9.4 ^c	-0.31 ± 12.40 ¹	35.0 ± 0.9	-6.1 ± 0.2
Guo et al. (2015)	-1862.3 ± 7.8 ¹	-1970.0 ± 4.2^c	118 ± 12	-361 ± 12 ^c	25.8 ± 9.8 ^c	25.6 ± 3.9	-0.64 ± 12.40 ¹	24.73 ± 10.72 ^c	-4.34 ± 1.88
This work	-1867.6 ± 3.2^c	-1970.0 ± 4.2 ^c	136 ± 25 ^c	-344 ± 25 ¹	20.6 ± 5.2^c	25.6 ± 3.9	17 ± 31 ¹	30.0 ± 0.3	-5.25 ± 0.05

619 ^a calculated with auxiliary data given by Langmuir (1978)

620 ^b calculated with auxiliary data given by Hemingway (1982)

621 ^c calculated with auxiliary data given by Grenthe et al. (1992)

622 ¹ calculated internally with the Gibbs-Helmholtz equation

623

- 626
627 Amme, M., Wiss, T., Thiele, H., Boulet, P. and Lang, H. (2005) Uranium secondary phase
628 formation during anoxic hydrothermal leaching processes of UO₂ nuclear fuel. *J. Nucl. Mater.*
629 **341**, 209-223.
- 630 Appelo, C.A.J. and Postma, D. (1996) *Geochemistry, Groundwater and Pollution*. A.A. Balkema,
631 Rotterdam, the Netherlands.
- 632 Baker, R.J. (2014) Uranium minerals and their relevance to long term storage of nuclear fuels.
633 *Coordin. Chem. Rev.* **266–267**, 123-136.
- 634 Brookins, D.G. (1975) Coffinite-Uraninite Stability relations in Grants Mineral Belt, New-
635 Mexico. *B.-Am. Assoc. Petrol. Geol.* **59**, 905-905.
- 636 Bros, R., Hidaka, H., Kamei, G. and Ohnuki, T. (2003) Mobilization and mechanisms of
637 retardation in the Oklo natural reactor zone 2 (Gabon) - inferences from U, REE, Zr, Mo and
638 Se isotopes. *Applied Geochem.* **18**, 1807-1824.
- 639 Bruno, J., Casas, I. and Puigdomènech, I. (1991) The kinetics of dissolution of UO₂ under
640 reducing conditions and the influence of an oxidized surface layer (UO_{2+x}): Application of a
641 continuous flow-through reactor. *Geochim. Cosmochim. Acta* **55**, 647-658.
- 642 Burns, P.C., Ewing, R.C. and Navrotsky, A. (2012) Nuclear Fuel in a Reactor Accident. *Science*
643 **335**, 1184-1188.
- 644 Carbol, P., Wegen, D.H., Wiss, T. and Fors, P. (2012) 5.16 - Spent Fuel as Waste Material, in:
645 Konings, R.J.M. (Ed.), *Comprehensive Nuclear Materials*. Elsevier, Oxford, pp. 389-420.
- 646 Casas, I., de Pablo, J., Gimenez, J., Torrero, M.E., Bruno, J., Cera, E., Finch, R.J. and Ewing, R.C.
647 (1998) The role of pe, pH, and carbonate on the solubility of UO₂ and uraninite under
648 nominally reducing conditions. *Geochim. Cosmochim. Acta* **62**, 2223-2231.
- 649 Castro, R.H.R. (2013) On the thermodynamic stability of nanocrystalline ceramics. *Mater. Lett.*
650 **96**, 45-56.
- 651 Clavier, N., Szenknect, S., Costin, D.T., Mesbah, A., Poinssot, C. and Dacheux, N. (2014) From
652 thorite to coffinite: A spectroscopic study of Th_{1-x}U_xSiO₄ solid solutions. *Spectrochim. Acta*
653 **A118**, 302-307.
- 654 Clavier, N., Szenknect, S., Costin, D.T., Mesbah, A., Ravaux, J., Poinssot, C. and Dacheux, N.
655 (2013) Purification of uranothorite solid solutions from polyphase systems. *J.Nucl. Mater.* **441**,
656 73-83.
- 657 Costin, D.T., Mesbah, A., Clavier, N., Dacheux, N., Poinssot, C., Szenknect, S. and Ravaux, J.
658 (2011) How To Explain the Difficulties in the Coffinite Synthesis from the Study of
659 Uranothorite? *Inorg. Chem.* **50**, 11117-11126.
- 660 Cox, J.D., Wagman, D.D. and Medvedev, V.A. (1989) *CODATA Key Values for*
661 *Thermodynamics*. Hemisphere Publ. Corp., New York.
- 662 Cuney, M. (1978) Geologic environment, Mineralogy, and fluid Inclusions of the Bois-Noirs-
663 Limouzat Uranium Vein, Forez, France. *Econ. Geol.* **73**, 1567-1610.
- 664 Dacheux, N., Brandel, V. and Genet, M. (1995) Synthèse et caractérisation de l'orthophosphate
665 d'uranium a valence mixte: U (UO₂)(PO₄)₂. *New J. Chem.* **19**, 15-26.
- 666 Deditius, A.P., Pointeau, V., Zhang, J.M.M. and Ewing, R.C. (2012) Formation of nanoscale Th-
667 coffinite. *Am. Mineral.* **97**, 681-693.

668 Deditius, A.P., Utsunomiya, S. and Ewing, R.C. (2008) The chemical stability of coffinite, USiO_4
669 $\cdot n\text{H}_2\text{O}$; $0 < n < 2$, associated with organic matter: A case study from Grants uranium region,
670 New Mexico, USA. *Chem. Geol.* **251**, 33-49.

671 Dreissig, I., Weiss, S., Hennig, C., Bernhard, G. and Zanker, H. (2011) Formation of
672 uranium(IV)-silica colloids at near-neutral pH. *Geochim. Cosmochim. Acta* **75**, 352-367.

673 Evins, L.Z. and Jensen, K.A. (2012) Review of spatial relations between uraninite and coffinite -
674 implications for alteration mechanisms. *MRS Online Proc. Library* **1475**, 89-96.

675 Ewing, R.C. (2015) Long-term storage of spent nuclear fuel. *Nature Mater.* **14**, 252-257.

676 Felmy, A.R., Cho, H., Rustad, J.R. and Mason, M.J. (2001) An aqueous thermodynamic model for
677 polymerized silica species to high ionic strength. *J. Sol. Chem.* **30**, 509-525.

678 Fleche, J.L. (2002) Thermodynamical functions for crystals with large unit cells such as zircon,
679 coffinite, fluorapatite, and iodoapatite from ab initio calculations. *Phys. Rev. B* **65**.

680 Frontera, C. and Rodriguez-Carvajal, J. (2003) FullProf as a new tool for flipping ratio analysis.
681 *Physica B* **335**, 219-222.

682 Fuchs, L.H. and Gebert, E. (1958) X-Ray Studies of Synthetic Coffinite, Thorite and
683 Uranothorites. *Am. Mineral.* **43**, 243-248.

684 Fuchs, L.H. and Hoekstra, H.R. (1959) The Preparation and Properties of Uranium(IV) Silicate
685 *Am. Mineral.* **44**, 1057-1063.

686 Gaucher, E.C., Tournassat, C., Pearson, F.J., Blanc, P., Crouzet, C., Lerouge, C. and Altmann, S.
687 (2009) A robust model for pore-water chemistry of clayrock. *Geochim. Cosmochim. Acta* **73**,
688 6470-6487.

689 Giffaut, E., Grivé, M., Blanc, P., Vieillard, P., Colàs, E., Gailhanou, H., Gaboreau, S., Marty, N.,
690 Madé, B. and Duro, L. (2014) Andra thermodynamic database for performance assessment:
691 ThermoChimie. *Applied Geochemistry* **49**, 225-236.

692 Gorman-Lewis, D., Burns, P.C. and Fein, J.B. (2008) Review of uranyl mineral solubility
693 measurements. *J. Chem. Thermodyn.* **40**, 335-352.

694 Grenthe, I., Fuger, J., Konings, R.J.M., Lemire, R.J., Muller, A.B., Nguyen-Trung, C. and
695 Wanner, H. (1992) Chemical Thermodynamics of Uranium. *Chemical Thermodynamics, 1*,
696 *OECD-NEA Eds* **1**, 715.

697 Guillaumont, R., Fanghänel, T., Neck, V., Fuger, J., Palmer, D.A., Grenthe, I. and Rand, M.H.
698 (2003) Update on the Chemical Thermodynamics of Uranium, Neptunium, Plutonium,
699 Americium and Technetium. *Chemical Thermodynamics, 5*, *OECD-NEA Eds*.

700 Gunnarsson, I. and Arnorsson, S. (2000) Amorphous silica solubility and the thermodynamic
701 properties of H_4SiO_4 degrees in the range of 0 degrees to 350 degrees C at P-sat. *Geochim.*
702 *Cosmochim. Acta* **64**, 2295-2307.

703 Guo, X., Szenknect, S., Mesbah, A., Labs, S., Clavier, N., Poinssot, C., Ushakov, S.V., Curtius,
704 H., Bosbach, D., Ewing, R.C., Burns, P.C., Dacheux, N. and Navrotsky, A. (2015)
705 Thermodynamics of formation of coffinite, USiO_4 . *Proceedings of the National Academy of*
706 *Sciences* **112**, 6551-6555.

707 Hemingway, B.S. (1982) Thermodynamic properties of selected uranium compounds and aqueous
708 species at 298.15K and 1 bar and at higher temperatures. Preliminary models for the origin of
709 coffinite deposits. *US. Geol. Survey Open-File Rep.* **82-619**, pp. 90.

710 Hoekstra, H.R. and Fuchs, L.H. (1956) Synthesis of Coffinite- USiO_4 . *Science* **123**, 105-105.

711 Hogselius, P. (2009) Spent nuclear fuel policies in historical perspective: An international
712 comparison. *Energ. Policy* **37**, 254-263.

713 Janeczek, J. (1999) Mineralogy and Geochemistry of Natural Fission Reactors in Gabon. *Revi.*
714 *Mineral.* **38**, 321-392.

715 Janeczek, J. and Ewing, R.C. (1992a) Coffinitization - A Mechanism for the Alteration of UO₂
716 under Reducing Conditions. *MRS Sympos. Proc.* **257**, 497-504.

717 Janeczek, J. and Ewing, R.C. (1992b) Dissolution and alteration of uraninite under reducing
718 conditions. *J. Nucl. Mater.* **190**, 157-173.

719 Jensen, K.A. and Ewing, R.C. (2001) The Okelobondo natural fission reactor, southeast Gabon:
720 Geology, mineralogy, and retardation of nuclear-reaction products. *Geol. Soc. Am. Bull.* **113**,
721 32-62.

722 Jerden Jr, J.L. and Sinha, A.K. (2003) Phosphate based immobilization of uranium in an oxidizing
723 bedrock aquifer. *Applied Geochem.* **18**, 823-843.

724 Johnson, J.W., Oelkers, E.H. and Helgeson, H.C. (1992) SUPCRT92 - A Software Package for
725 Calculating the Standard Molal Thermodynamic Properties of Minerals, Gases, Aqueous
726 Species, and Reactions from 1 Bar to 5000 Bars and 0°C to 1000°C. *Comput. Geosci.* **18**, 899-
727 947.

728 Labs, S., Hennig, C., Weiss, S., Curtius, H., Zanker, H. and Bosbach, D. (2014) Synthesis of
729 Coffinite, USiO₄, and Structural Investigations of U_xTh_(1-x)SiO₄ Solid Solutions. *Environ. Sci.*
730 *Technol.* **48**, 854-860.

731 Langmuir, D. (1978) Uranium Solution-Mineral Equilibria at Low-Temperatures with
732 Applications to Sedimentary Ore-Deposits. *Geochim. Cosmochim. Acta* **42**, 547-569.

733 Langmuir, D. and Chatham, J.R. (1980) Groundwater prospecting for sandstone-type uranium
734 deposits: a preliminary comparison of the merits of mineral-solution equilibria, and single-
735 element tracer methods. *J. Geochem. Exploration* **13**, 201-219.

736 Langmuir, D. (1997) Aqueous Environmental Geochemistry. Printice Hall Inc., New Jersey.

737 Maher, K., Bargar, J.R. and Brown, G.E. (2012) Environmental Speciation of Actinides. *Inorg.*
738 *Chem.* **52**, 3510-3532.

739 Mazeina, L., Ushakov, S.V., Navrotsky, A. and Boatner, L.A. (2005) Formation enthalpy of
740 ThSiO₄ and enthalpy of the thorite -> huttonite phase transition. *Geochim. Cosmochim. Acta*
741 **69**, 4675-4683.

742 Matzke, H. (1992) Radiation damage-enhanced dissolution of UO₂ in water. *J.Nucl. Mater.* **190**,
743 101-106.

744 Mercadier, J., Cuney, M., Cathelineau, M. and Lacorde, M. (2011) U redox fronts and
745 kaolinisation in basement-hosted unconformity-related U ores of the Athabasca Basin
746 (Canada): late U remobilisation by meteoric fluids. *Miner. Deposita* **46**, 105-135.

747 Mesbah, A., Szenknect, S., Clavier, N., Poinssot, C., Ewing, R.C. and Dacheux, N. (2015)
748 Coffinite, USiO₄, is abundant in nature: So why is it so difficult to synthesize? *Inorg. Chem.*
749 **54**, 6687-6696.

750 Min, M.Z., Fang, C.Q. and Fayek, M. (2005) Petrography and genetic history of coffinite and
751 uraninite from the Liueyiqi granite-hosted uranium deposit, SE China. *Ore Geol. Rev.* **26**, 187-
752 197.

753 Neck, V. and Kim, J.I. (2001) Solubility and hydrolysis of tetravalent actinides. *Radiochim. Acta*
754 **89**, 1-16.

755 Oelkers, E.H., Benezeth, P. and Pokrovski, G.S. (2009) Thermodynamic Databases for Water-
756 Rock Interaction, in: Oelkers, E.H., Schott, J. (Eds.), *Thermodynamics and Kinetics of Water-
757 Rock Interaction*, pp. 1-46.

758 Parkhurst, D.L. and Appelo, C.A.J. (1999) User's Guide to PHREEQC (Version 2) - A Computer
759 Program for Speciation, Batch-Reaction, One-Dimensional Transport, and Inverse
760 Geochemical Calculations. *U.S.G.S Water-Resources Investigations Report 99-4259*.

761 Parks, G.A. and Pohl, D.C. (1988) Hydrothermal solubility of uraninite. *Geochim. Cosmochim.*
762 *Acta* **52**, 863-875.

763 Peketroukhine, V., Riglet-Martial, C., Capdevila, H., Calmon, V., Bienvenu, P. and Laszak, I.
764 (2002) Effect of Soluble Silicates on the Solubility of Thorium(IV) Hydrous Oxide. *J. Nucl.*
765 *Sci. Technol.* **39**, 516-519.

766 Poinssot, C., Ferry, C., Lovera, P., Jegou, C. and Gras, J.-M. (2005) Spent fuel radionuclide
767 source term model for assessing spent fuel performance in geological disposal. Part II: Matrix
768 alteration model and global performance. *J. Nucl. Mater.* **346**, 66-77.

769 Pointeau, V., Deditius, A., Miserque, F., Renock, D., Becker, U., Zhang, J., Clavier, N., Dacheux,
770 N., Poinssot, C. and Ewing, R. (2009) Synthesis and characterization of coffinite. *J. Nucl.*
771 *Mater.* **393**, 449-458.

772 Pownceby, M.I. and Johnson, C. (2014) Geometallurgy of Australian uranium deposits. *Ore Geol.*
773 *Rev.* **56**, 25-44.

774 Rai, D., Felmy, A.R. and Ryan, J.L. (1990) Uranium(IV) Hydrolysis Constants and Solubility
775 Product of $\text{UO}_2 \cdot x\text{H}_2\text{O}(\text{am})$. *Inorg. Chem.* **29**, 260-264.

776 Rai, D., Yui, M. and Moore, D.A. (2003) Solubility and solubility product at 22 °C of $\text{UO}_2(\text{c})$
777 precipitated from aqueous U(IV) solutions. *J. Solution Chem.* **32**, 1-17.

778 Rai, D., Yui, M., Moore, D.A., Lumetta, G.J., Rosso, K.M., Xia, Y.X., Felmy, A.R. and
779 Skomurski, F.N. (2008) Thermodynamic model for $\text{ThO}_2(\text{am})$ solubility in alkaline silica
780 solutions. *J. Solution Chem.* **37**, 1725-1746.

781 Robie, R.A., Hemingway, B.S. and Fisher, J.R. (1979) Thermodynamic properties of minerals and
782 related substances at 298.15K and 1 bar pressure and at higher temperatures (revised edition).
783 *U.S. Geol. Survey Bull.* **1452**, 456 pp.

784 Schofield, E.J., Veeramani, H., Sharp, J.O., Suvorova, E., Bernier-Latmani, R., Mehta, A.,
785 Stahlman, J., Webb, S.M., Clark, D.L., Conradson, S.D., Ilton, E.S. and Bargar, J.R. (2008)
786 Structure of Biogenic Uraninite Produced by *Shewanella oneidensis* Strain MR-1. *Environ. Sci.*
787 *Technol.* **42**, 7898-7904.

788 Schuiling, R. D., Vergouwen, L., Vanderrijst, H. (1976) Gibbs energies of formation of zircon
789 (ZrSiO_4), thorite (ThSiO_4) and phenacite (Be_2SiO_4). *Am. Miner.*, **61**, 166-168.

790 Shilov, V.P., Yusov, A.B., Peretrukhin, V.F., Delegard, C.H., Gogolev, A.V., Fedosseev, A.M.
791 and Kazansky, L.P. (2007) Oxidation of U(IV) by atmospheric oxygen in pH 1.5–7.4 aqueous
792 solutions. *J. Alloy. Compd.* **444–445**, 333-338.

793 Stieff, L.R., Stern, T.W. and Sherwood, A.M. (1955) Preliminary Description of Coffinite - New
794 uranium Mineral. *Science* **121**, 608-609.

795 Stieff, L.R., Stern, T.W. and Sherwood, A.M. (1956) Coffinite, a Uranous Silicate with Hydroxyl
796 Substitution - A New Mineral. *Am. Mineral.* **41**, 675-688.

797 Stumm, W., Sigg, L. and Sulzberger, B. (1992) Chemistry of the Solid-Water Interface: Processes
798 at the Mineral-Water and Particle-Water Interface in Natural Systems. John Wiley & Sons, Inc.
799 pp. 428.

800 Szenknect, S., Costin, D.T., Clavier, N., Mesbah, A., Poinssot, C., Vitorge, P. and Dacheux, N.
801 (2013) From Uranothorites to Coffinite: A Solid Solution Route to the Thermodynamic
802 Properties of USiO_4 . *Inorg. Chem.* **52**, 6957-6968.

803 Thompson, P., Cox, D.E. and Hastings, J.B. (1987) Rietveld Refinement of Debye-Scherrer
804 Synchrotron X-Ray Data from Al₂O₃. *J. Appl. Crystallogr.* **20**, 79-83.
805 Ulrich, K.U., Singh, A., Schofield, E.J., Bargar, J.R., Veeramani, H., Sharp, J.O., Bernier-
806 Latmani, R. and Giammar, D.E. (2008) Dissolution of biogenic and synthetic UO₂ under
807 varied reducing conditions. *Environ. Sci. Technol.* **42**, 5600-5606.
808 White, A.F. (1995) Chemical Weathering Rates of Silicate Minerals in soils, in: White, A.F.,
809 Brantley, S.L. (Eds.), *Chemical Weathering Rates of Silicate Minerals*, Mineralogical Society
810 of America, Washington D.C., pp. 407-462.

811

812 ACKNOWLEDGMENT

813 Funding for this research was supported by the NEEDS Ressources program of the CNRS. EXAFS experiments were
814 performed with the financial support of the TALISMAN project. The authors are grateful to J. Ravaux and R. Podor
815 for ESEM and X-EDS analyses. The authors acknowledge Kastriot Spahiu (SKB) for his involvement in the
816 redaction, the helpful discussions and corrections made to the article. Support for RCE was provided by the U.S.
817 Department of Energy, Office of Science, Office of Basic Energy Sciences Energy Frontier Research Centers
818 program under Award Number DE-SC0001089.

819

820